

CC-VPSTO: Chance-Constrained Via-Point-based Stochastic Trajectory Optimisation for Safe and Efficient Online Robot Motion Planning

Lara Bruder Müller¹, Guillaume Berger², Julius Jankowski³, Raunak Bhattacharyya¹,
Raphaël Jungers² and Nick Hawes¹

Abstract—Safety in the face of uncertainty is a key challenge in robotics. We introduce a real-time capable framework to generate safe and task-efficient robot trajectories for stochastic control problems. We frame this as a chance-constrained optimisation problem constraining the probability of the controlled system to violate a safety constraint to be below a fixed threshold. To estimate this probability we propose a Monte-Carlo approximation. We suggest several ways to construct the problem given a fixed number of uncertainty samples, such that it is a reliable over-approximation of the original problem, i.e. any solution to the sample-based problem adheres to the original chance-constraint with high confidence. To solve the resulting problem, we integrate it into our motion planner VP-STO and name the enhanced framework Chance-Constrained (CC)-VPSTO. The strengths of our approach lie in i) its generality, without assumptions on the underlying uncertainty distribution, system dynamics, cost function, or the form of inequality constraints; and ii) its applicability to MPC-settings. We demonstrate the validity and efficiency of our approach on both simulation and real-world robot experiments.

Index Terms—Chance-Constrained Optimisation, Stochastic Model Predictive Control, Trajectory Optimisation

I. INTRODUCTION

Uncertainty is an inherent property of most real-world robotics applications. As robots are increasingly being deployed in safety-critical applications, *safety in the face of uncertainty* is an important research area in robotics. When considering the motion of a robot such as pictured in Figure 1, safe robot behavior is linked to the existence of a motion plan and underlying controller that achieves a given task while adhering to safety constraints. Safe behaviour must also take into account uncertainties in the environment, dynamics, and sensor measurements. Safety constraints can, for instance, address potential collisions, interaction forces, joint limits, or kinodynamic constraints. Many approaches from control theory,

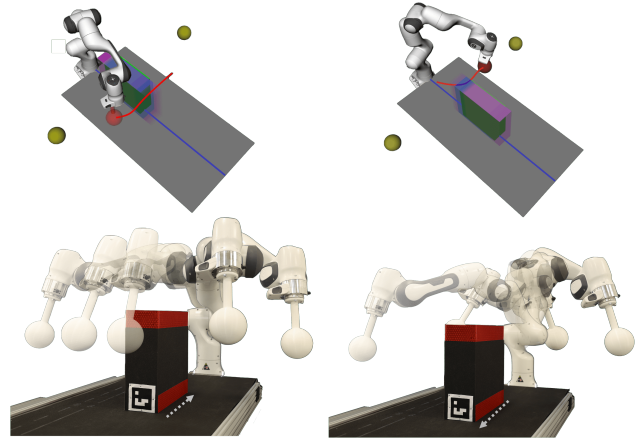


Fig. 1. *Real-robot experiment.* The robot is tasked to move its ball-shaped end effector from a start point on one side to a goal point on the other side of a conveyor belt (indicated by the yellow balls in the right simulation view). Meanwhile, the ball end effector has to avoid the box obstacle on a moving conveyor belt which is controlled according to a stochastic policy. Depending on the anticipated box movement, the robot can either pass the box in front (left images) or behind (right images). This problem setting requires the robot to be *reactive* whilst being able to plan *safe* motions in real-time. It further poses a trade-off between safety and performance, i.e., reaching the other side of the conveyor belt in minimum time.

such as robust control, address the problem of safe behaviour under uncertainty. However, these approaches typically assume that the uncertainty is bounded and optimise for the worst case. This is often unrealistic, or requires overly conservative bounds, resulting in suboptimal performance. In many cases, uncertainty is better modeled as a *probability distribution* over the environment configurations, with safety defined as a *low probability of constraint violation*. This has motivated the development of *chance-constrained optimisation*, which aims at finding solutions that are feasible with respect to constraints with high probability [1], [2].

A core advantage of chance-constrained formulations is their flexibility, making them suitable for a wide range of uncertainty models [3], [4]. Moreover, they offer a technique to balance between performance (e.g., the efficiency of a motion trajectory) and risk tolerance (i.e., the probability of constraint violation). Unfortunately, in general chance-constrained optimisation problems are challenging to solve exactly, and in the worst case intractable. In some cases the evaluation of the chance constraint alone may be intractable [5]. However, given an appropriate approximation of the chance constraint, a deterministic surrogate problem can be formulated and solved using standard optimisation techniques. Motivated by

For additional material, including the supplementary video, please visit <https://sites.google.com/oxfordrobotics.institute/cc-vpsto>.

¹ Oxford Robotics Institute, University of Oxford, UK; {larab, raunak, nickh}@robots.ox.ac.uk

² ICTEAM, UCLouvain, Belgium; {guillaume.berger, raphael.jungers}@uclouvain.be

³ Idiap Research Institute, Martigny and Ecole Polytechnique Fédérale de Lausanne (EPFL), CH; julius.jankowski@idiap.ch

LB was supported by an Amazon Web Services Lighthouse scholarship. JJ was supported by the Swiss National Science Foundation (SNSF) through the CODIMAN project. NH received EPSRC funding via the “From Sensing to Collaboration” programme grant [EP/V000748/1]. GB was supported by a “Wallonie-Bruxelles International” (WBI) grant and by a “Fonds de la Recherche Scientifique” (FNRS) fellowship. RJ is a FNRS honorary Research Associate. This project has received funding from the European Research Council (ERC) under the European Union’s Horizon 2020 research and innovation programme under grant agreement No 864017 - L2C.

the above, our work contributes a *tractable approximation of chance-constrained optimisation problems* suitable for robotics applications. We propose a Monte–Carlo approach that derives a deterministic surrogate problem to the stochastic chance-constrained problem from samples of the uncertainty. The primary considerations for this approach are: *i)* selecting the number of samples used in the Monte–Carlo approximation, *ii)* estimating the confidence in the validity of a solution to the surrogate problem with respect to the true chance constraint, and *iii)* devising an efficient solution method for the resulting deterministic problem.

The main contributions of this article are:

- 1) A Monte–Carlo (aka. sample-based) approach to chance-constrained robot motion planning problems, and we show that the resulting deterministic problem can be solved efficiently with the motion planner VP-STO [6].
- 2) Theoretical and empirical guarantees on the correctness of the this approach: namely, given a confidence level (*e.g.*, 95%), we guarantee with that confidence that the solution obtained from the surrogate problem satisfies the true chance constraint, *i.e.*, the chance constraint that is intractable or hard to solve analytically.
- 3) A problem formulation for chance-constrained motion planning that can be used for Model Predictive Control (MPC). By combining 1) and 2), this provides a tractable Monte–Carlo approach for safe real-time robot control.
- 4) Evaluations of the validity and efficiency of our approach in simulation studies for a 2D robot navigation problem with stochastic dynamic obstacles, and in real-world experiments on a Franka Emika robot arm.

The core advantages of this approach are: *i)* its flexibility, since a sample-based approach is able to handle arbitrary uncertainty models; *ii)* its real-time applicability within a receding-horizon scheme, including parallelisation; and last, *iii)* its ability to handle any type of inequality constraint within a chance constraint, *e.g.*, collision avoidance, bounded interaction forces, but also performance constraints, such as goal reaching.

II. RELATED WORK

Our work contributes to the domain of stochastic optimisation applied to Model Predictive Control (MPC), situated under the umbrella of *stochastic* MPC (SMPC). This paradigm seeks to solve optimal control problems for stochastic systems using a receding horizon approach. The stochasticity can manifest either as: system uncertainty, such as external disturbances, stochastic dynamics and sensor noise; or as model uncertainty. Given this stochasticity, achieving constraint satisfaction with absolute certainty is unattainable. Hence, one approach to SMPC is to formulate safety requirements as *chance constraints*. We refer to [7], [8] for a comprehensive survey of SMPC in a general setting. In the following, we provide a brief overview of model-based stochastic control approaches in the field of online robot motion planning under uncertainty. We note, that in this context, a key component in any algorithm is the ability to efficiently and reliably evaluate the probability of constraint violation. However, exact

evaluation of the chance of constraint satisfaction is typically intractable, and thus, has primarily been addressed through approximations. In the following, we distinguish between two main approaches: *sample-based* and *analytical* methods.

In the sample-based setting we can distinguish between *scenario optimisation* [4], [9] and *Monte–Carlo* methods [5], [10], [11]. Both use samples (aka. scenarios) of the uncertainty. Monte–Carlo methods typically approximate the probability of constraint violation from the samples. On the other hand, scenario optimisation synthesises a control satisfying the constraint for each of the samples. Scenario optimisation relies on a well-established theory of how many samples are needed to ensure chance constraint satisfaction with high confidence, *i.e.*, identifying the right sample size for a given confidence level (originally shown in the work of [12]). However, these theoretical bounds are mostly limited to convex or quasi-convex problems [13], [14] and solutions are still typically overly conservative, *i.e.*, they require much larger sample sizes than identified by empirical tests [4]. In contrast, Monte–Carlo methods are generally less conservative and share the advantage of coping with generic problems. However, they do not provide a finite-sample guarantee, but only asymptotic guarantees [11], implying the requirement of large sample sets, and higher computational resources. The need for large sample sets is reinforced when the desired probability of constraint violation is low, as is commonly targeted in robotics applications. A remedy to this can be the use of importance sampling [10], or data reduction methods based on parameter estimation of sample statistics, *e.g.*, through computing moments of the probability distribution of the uncertainty [15], [16], [17], [18]. Yet, the propagation of moments can be complex, and requires restrictive assumptions, such as Gaussianity. In contrast, our approach takes a different route by allowing for small sample sets, while adjusting the threshold for constraint violation based on the number of samples and the associated confidence bound, using tools from statistical learning.

Analytical methods are typically based on tractable convex approximations, *e.g.*, via conditional Value-at-Risk (CVaR) [19], semidefinite programming formulations [20] or constraint tightening [21], [22], [23]. Such methods have proven to be effective in providing probabilistic guarantees on the satisfaction of chance constraints, but are typically tailored to very specific types of constraints, uncertainty distributions and/or system dynamics, thereby limiting their applicability to real robotics problems.

Besides the distinction between sample-based and analytical methods, we also note that constraint violation probabilities can either be formulated *pointwise*, *i.e.*, independently for each time step, or *jointly*, *i.e.*, over the entire (finite) time horizon. This is important for robotics applications, where we are interested in robots being safe over the entire trajectory, *i.e.*, having a low joint probability of constraint violation. It is possible to bound the joint probability from the pointwise probabilities using an *additive* approach (using Boole’s inequality and summing over all pointwise probabilities, *e.g.*, [22], [16]) or a *multiplicative* one (multiplying the complement of all pointwise probabilities, *e.g.*, [24], [25]). Nevertheless, both approaches may lead to either an overestimation or

underestimation of the joint probability, as the pointwise probabilities are typically not fully independent [10], [9]. This further motivates the use of sample-based methods, since they offer the flexibility of working directly on either the joint or pointwise formulations, depending on the application.

The work of Yin et al. [26] is most similar to ours in terms of the proposed control architecture. Their risk-aware model predictive path integral (RA-MPPI) controller generates optimal control actions while imposing a bound on the *conditional Value-at-Risk* (CVaR) of the safety constraint. By using Monte–Carlo sampling to evaluate their risk metric within an MPPI controller, they achieve impressive MPC control rates in a racing scenario where the car’s dynamics are subject to various forms of noise. We use Monte–Carlo sampling to approximate a chance constraint, instead of a CVaR, and we similarly employ an optimisation scheme related to MPPI, called Covariance Matrix Adaptation Evolution Strategy (CMA-ES) [27]. The biggest difference between our work and RA-MPPI is that we account for the fact that we approximate a chance constraint using samples by including a confidence bound on the number of samples that violate the constraint. By contrast, RA-MPPI ignores possible errors in the approximation of the CVaR constraint.

In summary, our main observation across chance constrained optimisation approaches is that they are typically tailored to specific types of constraints (e.g., collision avoidance constraints, or reaching polytopic target sets) or specific types of uncertainty (e.g., Gaussian or bounded uncertainty). In contrast, we provide a general framework for chance-constrained finite-horizon optimal control problems with generic chance constraints and generic uncertainty distributions.

III. PROBLEM FORMULATION

A. Preliminaries

Let Δ be a random variable that models the uncertainty of the system. This can include stochasticity in the dynamics, the environment, and the sensor measurements. A realization δ of Δ will be referred to as an *uncertainty scenario*, or a *particle*. The probability distribution of Δ is denoted by $p_\Delta(\delta)$.

B. Chance-Constrained Optimisation

In the following, we introduce the general chance-constrained optimisation problem. The goal is to find a solution \mathbf{x} minimizing a cost $J(\mathbf{x})$ while satisfying a set of constraints. In our work, we consider inequality constraints, i.e., constraints that can be formulated as a function g being negative at \mathbf{x} , i.e., $g(\mathbf{x}) \leq 0$. For instance, g can encode a deterministic collision-avoidance constraint.

Chance-constrained optimisation generalises the above by allowing constraints that depend on a random variable. More precisely, the constraints have the form $g(\mathbf{x}, \delta) \leq 0$, where g depends on \mathbf{x} and the realization δ of the random variable Δ . For instance, $g(\mathbf{x}, \delta) \leq 0$ can encode a collision-avoidance requirement in a particular realisation, parameterised by δ , of a stochastic system and environment. Requiring that $g(\mathbf{x}, \delta) \leq 0$ holds for *all* realizations of δ is often overly conservative, or even infeasible. Therefore, chance-constrained optimisation

relaxes the constraint into a soft constraint, allowing violations of the constraint only with a probability, i.e., that the probability of sampling a δ that renders $g(\mathbf{x}, \delta) > 0$ is smaller than η . A general chance-constrained optimisation problem is as follows:

$$\begin{aligned} \min_{\mathbf{x} \in X} \quad & J(\mathbf{x}) \\ \text{s.t.} \quad & P_{\delta \sim \Delta} [g(\mathbf{x}, \delta) > 0] \leq \eta, \end{aligned} \quad (1)$$

where \mathbf{x} is the decision variable, constrained in some domain X , $J : X \rightarrow \mathbb{R}$ is the objective function, and $\eta \in [0, 1]$ is a user-provided threshold for the probability of violating g . We assume that the probability distribution p_Δ is known or that we have a generative model for p_Δ from which we can sample δ . We assume we can draw an arbitrary number of independent samples from this distribution, $\delta_1 \sim p_\Delta, \dots, \delta_N \sim p_\Delta$.

As mentioned above, the chance constraint is satisfied at \mathbf{x} if the probability of violating the constraint g at \mathbf{x} is lower than or equal to η . Computing this probability for a given \mathbf{x} is often challenging. For this reason, chance-constrained optimisation problems are often very hard, if not impossible, to solve exactly. Therefore we provide a tractable approximation of such problems, along with guarantees on the feasibility of the approximate solution with respect to the original chance constraint.

Note that Eq. (1) can be generalized to multiple constraints g_i , for $i = 1, \dots, m$, with different violation thresholds η_i . However, in this work, we will focus on a single constraint ($m = 1$) for simplicity.

C. Constraint Satisfaction as a Binary Random Variable

In this subsection, we reformulate the chance constraint in Eq. (1) as a constraint on a binary random variable obtained from Δ . Concretely, given \mathbf{x} , we introduce a random variable $G_{\mathbf{x}}$ with value in $\{0, 1\}$ that depends on Δ as follows: for any δ , if $\Delta = \delta$, then $G_{\mathbf{x}} = 1$ if the constraint g at \mathbf{x} with δ is violated; otherwise, $G_{\mathbf{x}} = 0$, i.e.,

$$P(G_{\mathbf{x}} = 1 \mid \Delta = \delta) = \begin{cases} 1 & \text{if } g(\mathbf{x}, \delta) > 0, \\ 0 & \text{otherwise.} \end{cases} \quad (2)$$

In the following, we write G instead of $G_{\mathbf{x}}$ when \mathbf{x} is clear from the context. Note that G is deterministic if the value of Δ is fixed. However, since Δ is a random variable, G is a random variable, too. Thus, we are interested in the probability distribution of the value of G . This can be obtained given a *known* probability distribution p_Δ of Δ , as follows:

$$P(G = 1) = \int_D P(G = 1 \mid \Delta = \delta) p_\Delta(\delta) d\delta, \quad (3)$$

wherein the integration domain D is all possible realizations δ of Δ . Using Eq. (3), the chance constraint in Eq. (1) can then be rewritten as

$$P(G_{\mathbf{x}} = 1) \leq \eta. \quad (4)$$

IV. MONTE-CARLO APPROXIMATION

Computing the probability in Eq. (4) can be challenging, because it requires integration over a possibly high-dimensional domain. Consequently, an appropriate approximation is required. A popular approach is the *particle-based* approximation proposed by Blackmore et al. [5]. The core concept is to draw a finite set of i.i.d. uncertainty samples, or particles, and approximate the integral in Eq. (3) as an average over the particles. This approach is justified by the law of large numbers: as the number of particles tends to infinity, the average converges to the true probability. In the remainder of this work, we refer to this kind of approximation as a *Monte-Carlo approximation*.

Formally, consider a set of N i.i.d. particles $\{\delta_i\}_{i=1}^N$ drawn from p_Δ . Based on $\{\delta_i\}_{i=1}^N$, a Monte-Carlo approximation of the integral in Eq. (3) can be computed as follows:

$$P(G = 1) \approx \frac{1}{N} \sum_{i=1}^N P(G = 1 \mid \Delta = \delta_i) \triangleq \frac{k}{N}. \quad (5)$$

This is equivalent to counting the number k of particles δ_i in $\{\delta_i\}_{i=1}^N$ that violate the constraint g at \mathbf{x} and dividing it by the total number of particles N . Note that given \mathbf{x} and δ , determining whether $g(\mathbf{x}, \delta) \leq 0$ and thus computing k for a given solution \mathbf{x} is generally much cheaper than computing the integral in Eq. (3).

To use Eq. (5) in the optimisation problem Eq. (1), we must construct a surrogate deterministic optimisation problem. A naive approach is to simply replace $P(G = 1)$ by its approximation, *i.e.*, requiring that $\frac{k}{N} \leq \eta$ at \mathbf{x} . In the remainder, we write this constraint as a bound on the number of particles in violation, *i.e.*, $k \leq \eta N$. When the number of samples approaches infinity, the solution to this approach asymptotically converges to the original chance constraint as depicted in Eq. (1). However, when using a finite set of particles, the Monte-Carlo approximation does not guarantee that the real chance constraint is satisfied at \mathbf{x} . Thus, we need to account for the gap between the true and the approximate probability. This is achieved by strengthening the constraint on the approximate probability. Therefore, instead of asking for $k \leq \eta N$, as in the naive approach, we require that $k \leq k_{\text{thresh}}$ for some $k_{\text{thresh}} < \eta N$. The precise value of k_{thresh} depends on the number of particles N and the desired *confidence* $1 - \beta$ that a solution \mathbf{x} satisfying $k \leq k_{\text{thresh}}$ satisfies the real chance constraint.

Confidence: The approximation in Eq. (5) comes from randomly sampled particles $\{\delta_i\}_{i=1}^N$. Hence, there is always a possibility that we sample a set of particles for which the approximation will be inaccurate, so that a solution \mathbf{x} may satisfy $k \leq k_{\text{thresh}}$ but not $P(G = 1) \leq \eta$. The *confidence* is the probability that we sample a good set of particles, *i.e.*, a set $\{\delta_i\}_{i=1}^N$ for which any solution \mathbf{x} satisfying $k \leq k_{\text{thresh}}$ satisfies $P(G = 1) \leq \eta$. Generally, a greater number of particles increases confidence for a specified k_{thresh} . The goal of the remainder of this section is to quantify the relation between the confidence, the threshold k_{thresh} , and the number of particles N .

A. Monte-Carlo Approximation as a Bernoulli Process

We note that the Monte-Carlo approximation of a chance constraint (Eq. (5)) can be considered as a Bernoulli process, *i.e.*, the act of drawing N samples from binary random variable G .

In a Bernoulli process, the number of samples with value one, denoted by K , follows a *Binomial distribution* [28], *i.e.*, for all $k \in \{0, \dots, N\}$,

$$P(K = k) = \binom{N}{k} p^k (1-p)^{N-k}, \quad (6)$$

wherein N is the total number of samples in the Bernoulli process, K is the random variable representing the number of outcomes with $G = 1$ and p is respective probability of an outcome of $G = 1$. Hence, we can express the probability of observing k constraint violations for the candidate solution \mathbf{x} among N particles in Eq. (5) by means of a Binomial distribution Eq. (6) with parameters N and $p = P(G = 1)$. This is an important insight as it yields a closed-form expression of *confidence* through the *cumulative distribution function (CDF)* $C(k; N, p)$ of the binomial distribution. This is the probability that $K \leq k$ when K follows a binomial distribution with parameters N and p :

$$C(k; N, p) = \sum_{\ell=0}^k \binom{N}{\ell} p^\ell (1-p)^{N-\ell}.$$

B. Confidence-bounded Surrogate Constraint

We now exploit the CDF of the binomial distribution in order to find a threshold k_β such that the chance constraint in Eq. (4) is satisfied with user-defined confidence $1 - \beta \in [0, 1]$ for any solution \mathbf{x} satisfying $k \leq k_\beta$. We refer to this as the *confidence-bounded surrogate constraint* to the original chance-constraint.

Proposition 1. *Let $\beta \in [0, 1]$ (typically, $\beta \ll 1$) and let k_β be an integer defined as follows:*

$$\begin{aligned} k_\beta &= \max \{k \in \mathbb{N} \mid C(k; N, \eta) \leq \beta\} \\ &\doteq C(\cdot; N, \eta)^{-1}(\beta). \end{aligned} \quad (7)$$

*Let $\mathbf{x}_{\text{reject}}$ be a solution that violates the chance constraint, *i.e.*, such that $P(G_{\mathbf{x}_{\text{reject}}} = 1) > \eta$, and let $\{\delta_i\}_{i=1}^N$ be a set of N independent samples from p_Δ . The following inequality holds:*

$$P\left(\sum_{i=1}^N P(G_{\mathbf{x}_{\text{reject}}} = 1 \mid \Delta = \delta_i) > k_\beta\right) \geq 1 - \beta. \quad (8)$$

The inequality in Eq. (8) describes the probability of correctly rejecting a candidate solution which will violate the constraint. Thus, we conclude that violating solutions are correctly rejected with a probability of at least $1 - \beta$. In other words:

Corollary 1. *If $\mathbf{x}_{\text{accept}}$ is such that the associated k in Eq. (5) satisfies $k \leq k_\beta$. Then, with confidence $1 - \beta$ w.r.t. the*

¹We move to k_β from k_{thresh} to emphasise its dependence on the confidence $1 - \beta$.

sampling of $\{\delta_i\}_{i=1}^N$, we can say that $\mathbf{x}_{\text{accept}}$ satisfies the chance constraint, i.e., $P(G_{\mathbf{x}_{\text{accept}}} = 1) \leq \eta$.

Proof of Proposition 1. Let $\mathbf{x}_{\text{reject}}$ be a solution that violates the chance constraint, i.e., $P(G_{\mathbf{x}_{\text{reject}}} = 1) \doteq p > \eta$. We look at the probability that $\mathbf{x}_{\text{reject}}$ is not rejected if we use $k_{\text{thresh}} = k_\beta$. This happens if and only if $\sum_{i=1}^N P(G_{\mathbf{x}_{\text{reject}}} = 1 \mid \Delta = \delta_i) \leq k_\beta$. Since $G_{\mathbf{x}_{\text{reject}}}$ is a binary random variable with probability p of having value one and $\{\delta_i\}_{i=1}^N$ are independent, the sum $\sum_{i=1}^N P(G_{\mathbf{x}_{\text{reject}}} = 1 \mid \Delta = \delta_i)$ follows a Binomial distribution with parameters N and p . Its CDF is thus $C(k; N, p)$. This implies that the probability that $\sum_{i=1}^N P(G_{\mathbf{x}_{\text{reject}}} = 1 \mid \Delta = \delta_i) \leq k_\beta$ is equal to $C(k_\beta; N, p)$. We now use the fact that the Binomial distribution is the monotonic with respect to p [28]: that is, $p_1 < p_2$ implies $C(k; N, p_1) > C(k; N, p_2)$. This implies that $\sum_{i=1}^N P(G_{\mathbf{x}_{\text{reject}}} = 1 \mid \Delta = \delta_i) \leq k_\beta$ is smaller than or equal to $C(k_\beta; N, \eta)$ since $p > \eta$. Now, by definition of k_β , it holds that $C(k_\beta; N, \eta) \leq \beta$, so that the probability of not rejecting $\mathbf{x}_{\text{reject}}$ is at most β . \square

In Fig. 2, we show the CDF of the binomial distribution for different values of N and p . From the plots, we can obtain k_β by looking at the intersection of the CDF with the horizontal line at $y = \beta$.

The key insight from the derivation of the above framework is that using the naive Monte–Carlo approach, i.e., $k_{\text{thresh}} = \eta N$, corresponds to a confidence $\beta \approx 0.5$. Indeed, in Fig. 2, we can see that $C(k; N, p)^{-1}(0.5) \approx pN$ because the horizontal line at $y = 0.5$ intersects the curves roughly at $k/N = p$. The naive approach is thus more optimistic than the confidence-bounded approach but it is in general a misplaced optimism because it results in a high probability ($\approx 50\%$) of accepting a infeasible candidate. This is further illustrated in Sec. B and Fig. 10 in the Appendix.

The idea of expressing a chance constraint in terms of a deterministic predicted variable K and the inverse CDF $k_\beta = \text{CDF}^{-1}(\beta)$ is not new; see, e.g., [7]. In fact, it has been used in the past to derive theoretical bounds on the number of samples needed to ensure constraint satisfaction in scenario optimisation approaches; see, e.g., [29]. Yet, to the best of our knowledge, it has never been used within the Boolean formulation of a chance constraint and its the Monte–Carlo approximation. Instead, it has only been used for simple continuous constraints with tractable distributions for which the CDF could be derived analytically.

V. CHANCE-CONSTRAINED VP-STO

Building upon our previous trajectory optimisation framework *VP-STO* [6], we introduce *chance-constrained VP-STO (CC-VPSTO)* for finding robot trajectories that minimise a given task-related objective *while satisfying a given chance constraint*. Hence, for the remainder of the paper, the decision variable \mathbf{x} for the problem presented in Eq. (1) is a set of via-points $\mathbf{q}_{\text{via}} = (q_{\text{via},1}, \dots, q_{\text{via},m})$, i.e., $\mathbf{x} = \mathbf{q}_{\text{via}}$.

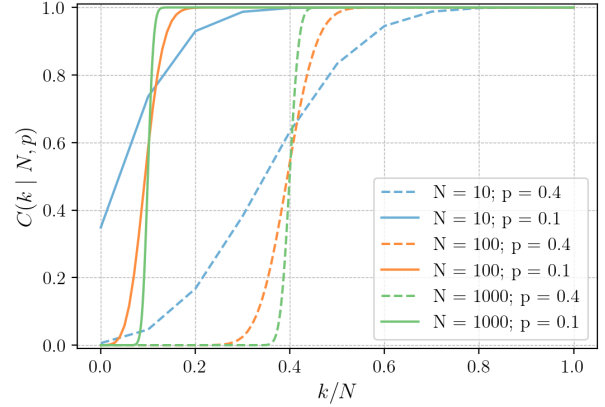


Fig. 2. CDF of the binomial distribution for different values of N and p , given k/N on the x-axis. The CDF values map to our confidence in observing k/N constraint violations under the assumption that the true probability of constraint violation is p .

Based on these via-points, we efficiently synthesise continuous trajectories $\xi = \{\mathbf{q}_{0:T}, \dot{\mathbf{q}}_{0:T}, \ddot{\mathbf{q}}_{0:T}, T\}$.²

We use the particle-based approximation in Eq. (5), and we enforce the associated constraint $k \leq k_{\text{thresh}}$ through a penalty-based approach, i.e., we include the constraint $k \leq k_{\text{thresh}}$ in the objective function as a penalty term. This can be seen as a discontinuous barrier function that adds a very high penalty term J_{pen} to the objective function if the constraint is violated, i.e., when the observed number of constraint violations $k > k_{\text{thresh}}$. The closed-form formulation of this penalty term is as follows:

$$J_{\text{pen}} = \mathbf{1}[k > k_{\text{thresh}}] \cdot (J_{\text{pen},\text{min}} + a \cdot (k - k_{\text{thresh}} - 1)).$$

We choose the minimum penalty term $J_{\text{pen},\text{min}}$ to be much larger than the maximum cost objective without constraint violations. Moreover, we add a piecewise linear term to the minimum penalty term that grows linearly with the extra number of violations compared to k_{thresh} . This term makes the constraint landscape smoother and gives the optimiser a direction towards feasible solutions without violations. The overall algorithm for CC-VPSTO is summarised in Alg. 1, where the approximation of the chance constraint, i.e., counting the number of particles that cause the solution to violate the constraint, is encapsulated in the `evaluate` function.

In our previous work, we demonstrated the suitability of the VP-STO framework for real-time robot motion planning in dynamic environments [6]. Similarly, the CC-VPSTO framework, i.e., the above algorithm, can be used in a receding horizon MPC scheme to generate robot trajectories in real-time. Yet, we note that the constraint evaluation in the `evaluate` function will be computationally more expensive than in the original VP-STO framework, as it requires N Monte–Carlo simulations per candidate trajectory ξ . This implies that the reactivity of our framework now depends on the number of particles N used for the approximation. The advantage of our heuristic is that we can choose the number of samples used in the approximation then use confidence to reason about

²For more information on how we generate the continuous trajectories from via-points, we refer the reader to Sec. A in the Appendix and to [6], [30].

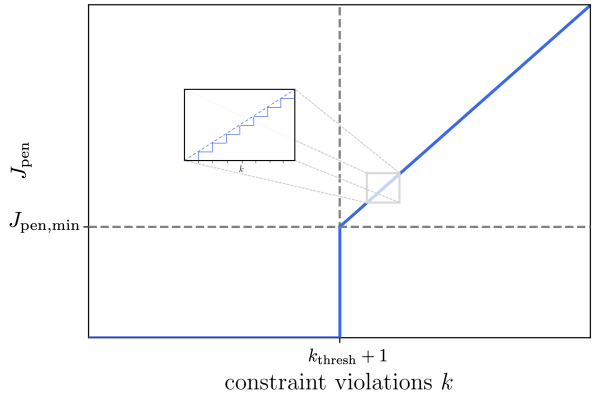


Fig. 3. Graph of the penalty function used in CC-VPSTO. When observing more than k_{thresh} constraint violations in the N Monte-Carlo simulations, the penalty function takes value $J_{\text{pen,min}}$ plus a quantity proportional to the number of extra constraint violations compared to k_{thresh} . Note that we chose the minimum penalty term $J_{\text{pen,min}}$ to be much larger than the largest cost objective without constraint violations.

Algorithm 1: CC-VPSTO

Input: $q_0, \dot{q}_0, q_T, \dot{q}_T, \dot{q}_{\min}, \dot{q}_{\max}, \ddot{q}_{\min}, \ddot{q}_{\max}, N_{\text{via}}, \text{maxIter}, M, H, \eta, \beta, N$

/ N_{via} : no. of via-points, */*
/ maxIter : max. no. of CMA-ES iterations, */*
/ M : no. of sampled candidate trajts. */*
/ H : horizon */*
/ η : chance constraint threshold */*
/ β : confidence threshold */*
/ N : no. of particles */*

Output: Robot trajectory $\xi_{0:H}^*$

${}^0\mu_{\text{via}}, {}^0\Sigma_{\text{via}} \leftarrow \text{init}(N_{\text{via}})$
 $j \leftarrow 0$
 Sample $\Delta \leftarrow \{\delta_i \sim p_{\Delta}\}_{i=1}^N$
 $k_{\beta} \leftarrow C(k | N, \eta)^{-1}(\beta)$
while $j < \text{maxIter}$ **do**
 $\{q_{\text{via}}\}_{m=1}^M \leftarrow \text{sample}({}^j\mu_{\text{via}}, {}^j\Sigma_{\text{via}})$ // via-points
 $\{\xi\}_{m=1}^M \leftarrow \text{synthesise}(\{q_{\text{via}}\}_{m=1}^M)$ // trajectories
 $\{c\}_{m=1}^M \leftarrow \text{evaluate}(\{\xi\}_{m=1}^M, k_{\beta}, \Delta)$ // cost
 $\mu_{\text{via}}^{j+1}, \Sigma_{\text{via}}^{j+1} \leftarrow \text{CMA-ES}(\{q_{\text{via}}, c\}_{m=1}^M)$
 $j \leftarrow j + 1$
end
 $\xi_{0:H}^* \leftarrow \text{synthesise}(\mu_{\text{via}}^j)$

an appropriate threshold. In contrast, a scenario-optimisation approach is typically tied to a large number of samples, derived from conservative bounds. Instead, we can tie the choice of number of samples to the frequencies at which we want to run the MPC-scheme.

VI. PROPERTIES OF THE PROPOSED APPROXIMATION

As we have seen in the previous section, the proposed approximation is based on the Bernoulli process of sampling N particles from the distribution p_{Δ} and evaluating the constraint g for each particle. In this section, we provide a theoretical view on the proposed approximation and derive additional bounds on the probability of constraint violation for a given

candidate solution x in the particular problem setting of robot motion planning in a dynamic environment with ball-shaped obstacles.

A. Limitation of the Bernoulli Process

A crucial assumption in Proposition 1 is that the Bernoulli experiments $P(G_x = 1 | \Delta = \delta_i)$ for $i = 1, \dots, N$, are independent, so that their sum in Eq. (5) follows a Binomial distribution. However, although the samples $\{\delta_i\}_{i=1}^N$ themselves are independent, as x depends on these samples through the optimisation scheme, the values of $P(G_x = 1 | \Delta = \delta_i)$ for $i = 1, \dots, N$, are not independent. Instead, they are linked to each other via x . Hence, only under the assumption that x is independent from the samples $\{\delta_i\}_{i=1}^N$, the sum $\sum_{i=1}^N P(G_x = 1 | \Delta = \delta_i)$ follows a binomial distribution, and Proposition 1 holds. In the following, we sketch two scenarios where the assumption actually holds.

i) In the first scenario, we have a candidate solution x and we evaluate the violation probability of this candidate by using a different set of samples, *i.e.*, a set of samples that was not used to compute x . In our optimisation scheme, this implies that we resample after each iteration³ and use the new samples to evaluate the violation probability of the solution computed at the previous iteration (and if the violation probability is too large, then we can compute a new solution). However, this approach is computationally expensive and requires resampling after each iteration, which can impede convergence.

Nevertheless, for a class of safety constraints, coined as *separable* constraints, resampling is not needed because, even though x is computed from the samples, the sample sets that lead to an unsafe x are exactly those that incorrectly accept a fixed unsafe solution x_{fixed} . We are thus back to estimating the probability of violation of a fixed candidate solution, namely x_{fixed} . The separable constraints are the constraints $g(x, \delta) \leq 0$ of the form $h_1(x) \geq h_2(\delta)$ wherein h_1 and h_2 are real-valued functions and h_1 is continuous. A formal statement of the above result, as well as examples of collision-avoidance problems than can be formulated with separable constraints are given in Appendix C.

ii) Alternatively, in an iterative optimisation process, if after several iterations the solution does not change anymore, then the solution can be considered as fixed so that scenario *i)* applies. By extension, we claim that if the solution changes *only slightly* after several iterations, then in this case Proposition 1 can be used as an accurate heuristic. This happens for instance in an online MPC scheme for safe optimal control. In this case, the decision variable x_k , generated in one MPC-step k will be executed for a few milliseconds only, until we resample and recompute a new solution in the next MPC-step. At each step, the new solution is likely to be similar to the solution that was obtained at the previous step. Hence, if we look at the global solution, *i.e.*, the concatenation of all partial solutions

³This assumes that we use iterative or evolutionary algorithms to solve the chance-constrained optimisation problem.

$\{\mathbf{x}_k\}_{k=0}^T$ generated by the MPC-scheme, Proposition 1 can be used.

Despite identify applications where the independence assumption holds, we refer to the use of the confidence-bounded threshold k_β as a *heuristic* since it does not apply in all cases. For the remainder of the paper, we define $\eta_{\text{binom}} = k_\beta/N$. In the next subsection, we derive another threshold $k_{\beta,\text{rad}}$ which does not require the independence of the Bernoulli variables, but is limited to a specific motion planning problem. We present this to provide a point of contrast to k_β , with $k_{\beta,\text{rad}}$ being more theoretically complete but also more conservative and computationally expensive.

B. Theoretical Bounds for Obstacle Collision Avoidance

We consider a robot motion planning problem, wherein a ball-shaped robot has to avoid m ball-shaped obstacles with high probability across time instants t_1, \dots, t_H .

For the sake of simplicity, we first focus on the case with one obstacle ($m = 1$) and one time step ($H = 1$), before generalising. Thus, we consider the problem of finding the optimal position $\mathbf{q}(\mathbf{x}^*) \in \mathbb{R}^n$ of the center of the robot at time $t = t_1$, parameterised by the decision variable \mathbf{x} , such that $P_{\delta \sim \Delta}(\|\mathbf{q}(\mathbf{x}) - \mathbf{p}(\delta)\| \geq r) \geq 1 - \eta$, wherein $r \geq 0$ is the combined radius of the obstacle and the robot, and $\mathbf{p}(\delta) \in \mathbb{R}^n$ is the position of the center of the obstacle at time $t = t_1$ for the uncertainty sample δ . Thus, in the formulation of Eq. (1), $g(\mathbf{x}, \delta) = r - \|\mathbf{q}(\mathbf{x}) - \mathbf{p}(\delta)\|$ i.e., $g(\mathbf{x}, \delta) \leq 0 \Leftrightarrow \|\mathbf{q}(\mathbf{x}) - \mathbf{p}(\delta)\| \geq r$.

By using tools from statistical learning, we obtain a confidence bound on $P(G = 1)$ from the observed number of collisions k . To obtain this result, we use the *Rademacher complexity* of the set of functions $F = \{\delta \mapsto P(G_{\mathbf{x}} = 1 \mid \Delta = \delta) : \mathbf{x}\}$, defined for all N by

$$R_N(F) = E_{\delta_1, \dots, \delta_N} \left[E_{\sigma_1, \dots, \sigma_N} \left[\sup_{f \in F} \frac{1}{N} \sum_{i=1}^N \sigma_i f(\delta_i) \right] \right],$$

where $\{\delta_i\}_{i=1}^N$ are independent samples of p_Δ and $\{\sigma_i\}_{i=1}^N$ are sampled independently uniformly at random in $\{-1, 1\}$. A well-known result in statistical learning [31, Theorem 3.3] states that if $\{\delta_i\}_{i=1}^N$ is a set of N independent samples from p_Δ , then for any \mathbf{x} , it holds that

$$P \left(p \leq \frac{k}{N} + 2R_N(F) + \sqrt{\frac{\log(\frac{1}{\beta})}{2N}} \right) \geq 1 - \beta, \quad (9)$$

wherein $p = P(G_{\mathbf{x}} = 1)$, $k = \sum_{i=1}^N P(G_{\mathbf{x}} = 1 \mid \Delta = \delta_i)$ and $F = \{\delta \mapsto P(G_{\mathbf{x}} = 1 \mid \Delta = \delta) : \mathbf{x}\}$.

In Appendix D, we bound $R_N(F)$ as follows:

$$R_N(F) \leq \sqrt{\frac{d \log(\frac{eN}{d})}{2N}},$$

wherein $d = n + 1$ and e is Euler's number. By combining with Eq. (9), we obtain the following confidence bound on $P(G = 1)$:

Proposition 2. Let $\beta \in (0, 1]$ (typically, $\beta \ll 1$), and let $\{\delta_i\}_{i=1}^N$ be a set of N independent samples from p_Δ . Then, for any \mathbf{x} , it holds that

$$P \left(p \leq \frac{k}{N} + \sqrt{\frac{2d \log(\frac{eN}{d})}{N}} + \sqrt{\frac{\log(\frac{1}{\beta})}{2N}} \right) \geq 1 - \beta, \quad (10)$$

wherein $p = P(G_{\mathbf{x}} = 1)$, $k = \sum_{i=1}^N P(G_{\mathbf{x}} = 1 \mid \Delta = \delta_i)$ (where G accounts for the collision with one obstacle at one time step), $d = n + 1$ and e is Euler's number.

Proposition 2 tells us that if we define $k_{\beta,\text{rad}}$ as

$$k_{\beta,\text{rad}} = \max \left\{ k \in \mathbb{N} : \frac{k}{N} + \sqrt{\frac{2d \log(\frac{eN}{d})}{N}} + \sqrt{\frac{\log(\frac{1}{\beta})}{2N}} \leq \eta \right\},$$

then any solution for which $k \leq k_{\beta,\text{rad}}$, satisfies the chance constraint $P(G = 1) \leq \eta$ with confidence $1 - \beta$.

We now discuss the case of multiple ball-shaped obstacles ($m > 1$) and multiple time steps ($H > 1$). In this case, we show (see Appendix D) that $R_N(F)$ can be bounded as follows:

$$R_N(F) \leq \sqrt{\frac{d \log(\frac{eN}{d})}{2N}}.$$

Hence, we obtain the following result:

Proposition 3. Let $\beta \in (0, 1]$ (typically, $\beta \ll 1$), and let $\{\delta_i\}_{i=1}^N$ be a set of N independent samples from p_Δ . Then, for any \mathbf{x} , it holds that

$$P \left(p \leq \frac{k}{N} + mH \sqrt{\frac{2d \log(\frac{eN}{d})}{N}} + \sqrt{\frac{\log(\frac{1}{\beta})}{2N}} \right) \geq 1 - \beta, \quad (11)$$

wherein $p = P(G_{\mathbf{x}} = 1)$, $k = \sum_{i=1}^N P(G_{\mathbf{x}} = 1 \mid \Delta = \delta_i)$ (where G accounts for the collision with m obstacles at H time steps), $d = n + 1$ and e is Euler's number.

Proposition 3 tells us that if we define $k_{\beta,\text{rad}}$ as

$$k_{\beta,\text{rad}} = \max \left\{ k \in \mathbb{N} : \frac{k}{N} + mH \sqrt{\frac{2d \log(\frac{eN}{d})}{N}} + \sqrt{\frac{\log(\frac{1}{\beta})}{2N}} \leq \eta \right\},$$

then any solution for which $k \leq k_{\beta,\text{rad}}$, satisfies the chance constraint $P(G = 1) \leq \eta$ with confidence $1 - \beta$.

Note that unlike other approaches in the literature our confidence bound Eq. (11) does not use Boole's inequality to bound the joint probability of collision avoidance. Indeed, the use of Boole's inequality would us require to set the individual collision avoidance probability to $\bar{\eta} = \frac{\eta}{mH}$ and the associated

confidence to $1 - \bar{\beta}$ with $\bar{\beta} = \frac{\beta}{mH}$. This would result in $\bar{k}_{\beta, \text{rad}}$ as follows:

$$\bar{k}_{\beta, \text{rad}} = \max \left\{ k \in \mathbb{N} : \frac{k}{N} + \sqrt{\frac{2d \log\left(\frac{eN}{d}\right)}{N}} + \sqrt{\frac{\log\left(\frac{mH}{\beta}\right)}{2N}} \leq \frac{\eta}{mH} \right\}.$$

From this it is evident that $\bar{k}_{\beta, \text{rad}} \leq k_{\beta, \text{rad}}$.

VII. EXPERIMENTS

We evaluate our framework, *i.e.*, Algorithm 1, with and without the MPC-scheme, in simulations and a real-world experiment with a Franka Emika robot arm. The simulation experiments allow us to make claims about the empirical performance of our system across different settings and parameterisations. The robot experiment allows us to evaluate the real-time applicability of our approach. The supplementary video includes video recordings from the actual robot experiment along with a selection of video samples from the simulated experiments. These can also be found on our website <https://sites.google.com/oxfordrobotics.institute/cc-vpsto>.

A. A priori Clarifications & Terminology

1) *Joint probability of constraint violation*: In all our experiments the chance constraint tested is *high-probability collision avoidance*. We encode this as a *joint* chance constraint, *i.e.*, enforcing *trajectory-wise* constraint satisfaction with high probability. A joint formulation is the more meaningful interpretation for robot behaviour, in contrast to evaluating the safety constraint independently at each time step. This means that we would not consider a trajectory to be safe if it avoids collisions in one time step with a very high probability, but collides in the next time step. We thus consider correlation over time in the chance constraint, *i.e.*, the first collision in a trajectory renders the whole trajectory unsafe and all subsequent collisions do not add any additional risk. This is in contrast to the *point-wise* formulation of the chance constraint which does not consider the correlation over time.

2) *Particles*: Before we outline our experiments in more detail, we want to clarify our use of particles for *i)* our algorithm and *ii)* its evaluation. As outlined above, in our algorithm, we use particles to approximate the chance constraint in the optimisation scheme. Moreover, we also use particles to approximate the distribution of test environments the planned trajectory could encounter in the experiments. For both cases, the algorithm and the evaluation, the definition of a particle is the same: One particle always maps to one particular belief state of how the specific environment is going to evolve or looks like. In the case of one static uncertain obstacle, a particle would therefore directly map to the obstacle's position. While in the case of one dynamically moving obstacle, one particle would map to a trajectory, *i.e.*, the prediction of where that obstacle is going to be in the next time steps. And finally, in the case of multiple dynamic obstacles, one particle maps to M trajectory predictions for M obstacles. Thus, the general approach taken in each of the experiments is to first draw a

set of particles that we use within the optimisation scheme to generate a solution trajectory and then, second, to draw another set of particles from the same distribution, to evaluate the given solution.

3) *Collisions*: In the case of a single obstacle, we consider a robot trajectory to be in collision if the robot would collide with the obstacle at *any point in time*. For multiple obstacles, we extend this definition to say a robot trajectory is in collision if the robot would collide with *any* obstacle *at any point in time*. By this, we avoid double counting collisions. One particle can only be counted as one collision, even in cases where it might collide with several obstacles at different points in time.

B. Simulation Experiments

All simulation experiments are conducted in a bounded 2D environment with a circular holonomic robot, as shown in Fig. 5. In Section VII-B1 we perform offline planning experiments, where we run CC-VPSTO only once to compute a trajectory over the full horizon from start to goal. In Section VII-B3 we evaluate the online planning case, where we follow a receding horizon approach using CC-VPSTO to re-plan the trajectory at every MPC step. The results of the offline experiments will also be relevant for the online setting, as each online replanning step can be seen as solving a new offline optimisation problem. In both experiment settings, the uncertainty stems from obstacles in the environment, with no uncertainty in the robot dynamics⁴. For the offline planning case, we assume that the obstacles are static but we don't know their exact position, relating to measurement uncertainty. For the online receding horizon setting, we assume the obstacles are moving according to a random walk model. In addition, their velocities are inverted when they hit the boundaries, keeping them inside the workspace and rendering their dynamics non-linear. In all the experiments, the obstacles are assumed to be circular with different radii, but they could be replaced with more complex shapes, as we do not require any kind of convexity in our optimisation scheme.

1) *Offline Planning*: In order to show the properties of CC-VPSTO, we use a simple offline setting with a single static obstacle. The obstacle's uncertain position follows a Gaussian distribution⁵, as shown in Fig. 5. Therefore in this offline setting a particle, as explained in more detail in Section VII-A, refers to a possible (static) position of the obstacle.

For every combination of values of N (100, 1000) and η (0.05, 0.1, 0.15, 0.2, 0.25, 0.3, 0.35, 0.4, 0.6, 0.8), we run $N_{\text{exp}} = 10^5$ experiments. For $i = 0, \dots, N_{\text{exp}}$ sample sets of N i.i.d. particles, we compute the trajectory ξ_i using CC-VPSTO with $k_{\beta}(\beta, \eta, N)$. Then, for each trajectory ξ_i , we evaluate its probability $\hat{\eta}_i$ of colliding with the static uncertain obstacle. We use a new set of $N_{\text{eval}} = 10^4$ i.i.d. particles, sampled from the same distribution of possible obstacle locations, and count the number of particles that

⁴This is for simplicity only. The extension to process noise and external disturbances is straightforward given the proposed approach.

⁵Note, we do not exploit the fact that the position is Gaussian distribution. We could replace this with any other arbitrary distribution.

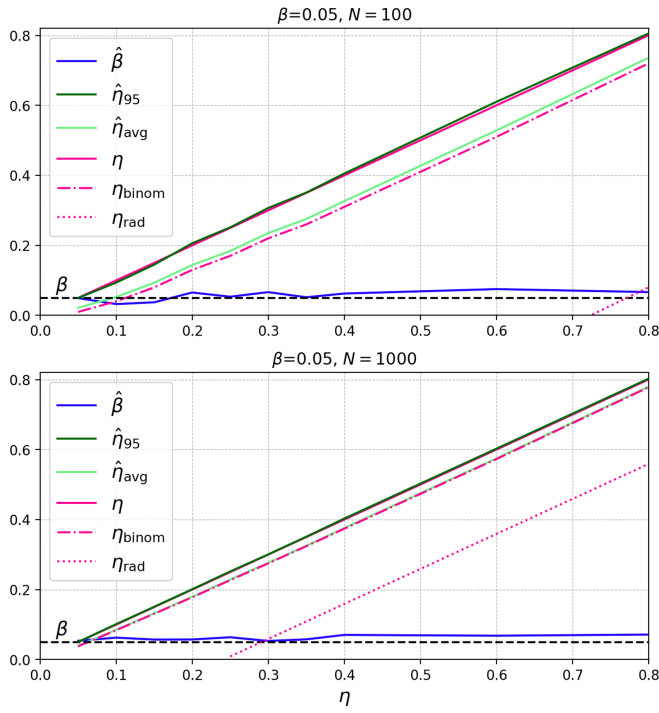


Fig. 4. **Offline Planning Experiment.** We evaluate the heuristic η_{binom} for different values of η and numbers of particles N (100, 1000) by running CC-VPSTO $N_{\text{exp}} = 10^5$ times and evaluating the solutions on a set of $N_{\text{eval}} = 10^4$ new unseen samples. We compare the heuristic η_{binom} to the Rademacher-complexity bound η_{rad} . We also show the mean collision probability $\hat{\eta}_{\text{avg}}$ and the $(1 - \beta)$ -percentile of the collision probabilities, *i.e.*, $\hat{\eta}_{(1-\beta)}$ across experiments. Last, we show the empirical probability of chance constraint violation $\hat{\beta}$, which is the share of experiments that had a collision probability $\hat{\eta}_i > \eta$.

collide with ξ_i . The ratio of this number by N_{eval} is $\hat{\eta}_i$. We use $\hat{\eta}_i$ to compute the following three metrics:

1) **Mean collision probability:**

$$\hat{\eta}_{\text{avg}} = \sum_{i=0}^{N_{\text{exp}}} \hat{\eta}_i / N_{\text{exp}}$$

2) **$(1-\beta)$ -percentile of the collision probability:**

$$\hat{\eta}_{(1-\beta)} = \text{percentile}(\{\hat{\eta}_i\}_{i=0}^{N_{\text{exp}}}, 1 - \beta)$$

3) **Probability of chance constraint violation:**

$$P(\hat{\eta}_i > \eta) = \hat{\beta} = \left(\sum_{i=0}^{N_{\text{exp}}} \mathbf{1}(\hat{\eta}_i > \eta) \right) / N_{\text{exp}}$$

Note, that we denote *empirical* values with a hat, *e.g.*, $\hat{\eta}$.

For the heuristic to be a good approximation, a share of maximum β of the solutions can be in collision. This is because we set our confidence threshold to $1 - \beta$, thereby permitting the acceptance of "poor" approximations in a fraction of β instances. A trajectory ξ_i is deemed to be in collision, *i.e.*, violate the chance constraint, if its estimated value $\hat{\eta}_i$ exceeds η . Besides the experiment results, we also provide the values of η_{binom} and η_{rad} obtained from the bounds derived from the Binomial distribution (our heuristic) and the Rademacher complexity.

Results: The numerical results of our offline analysis are summarised in Fig. 4. The pink dotted curves show the theoretical values of η_{binom} and η_{rad} , and the green curves show the empirical values of $\hat{\eta}_{\text{avg}}$ and $\hat{\eta}_{(1-\beta)}$. In addition, we plot the empirical probability of chance constraint violation $\hat{\beta}$ in blue against the user-defined value of β . The numbers from which we created the plots are also listed in Tab. II in

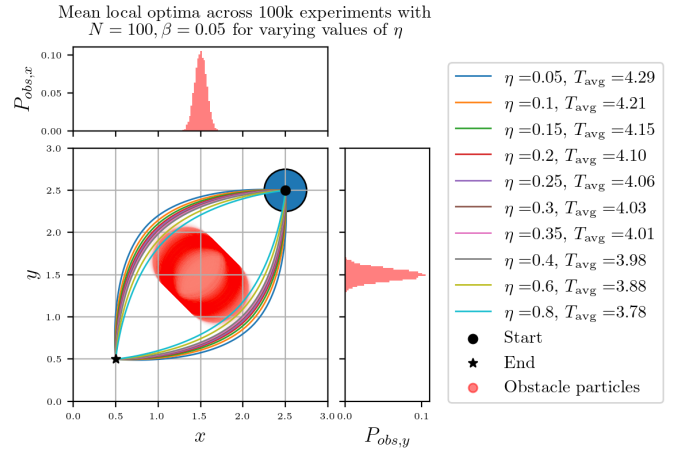


Fig. 5. **Offline Planning Experiment.** We show $N_{\text{eval}} = 10^4$ red circles for the uncertain obstacle position and the mean trajectory for the two local optima from CC-VPSTO, which used $N = 100$ particles in the optimisation, for varying values of η across $N_{\text{exp}} = 10^5$ experiments. The blue circle shows the robot's radius and starting position.

the Appendix. We also visualize the mean trajectories for the two local optima found by CC-VPSTO for different values of η in Fig. 5. Note, that we only show the solutions for the experiments with $N = 100$ in the optimisation, as the solutions for $N = 1000$ are visually indistinguishable. In the legend of Fig. 5, we also show the average motion duration of the trajectories across experiments for the different values of η . Quantitatively, from Fig. 4, we observe that the heuristic η_{binom} provides a good value for k_{thresh} since the observed $\hat{\eta}_{0.95}$ is close to the target η (or equivalently, $\hat{\beta}$ is close to β). This means that in practice the probability of collision is below η , with confidence 95%. We also observe that when N is larger, η_{binom} and $\hat{\eta}_{\text{avg}}$ are closer to η . This means that the surrogate optimisation problem becomes less conservative as the number of particles increases, given the same user-defined confidence-level. This is normal since more particles provide a better approximation of the distribution. The figure also shows that the Rademacher-complexity-based bound η_{rad} is much more conservative, as it is always smaller than η_{binom} . Moreover, the offset from η_{binom} increases substantially with a decreasing number of particles N . Qualitatively, we can see from Fig. 5 that with higher values of η , CC-VPSTO finds more efficient, but also less safe trajectories, as the mean trajectories are closer to the obstacle, since they allow for a higher probability of collision.

2) **Comparison between $k_{\beta, \text{rad}}$ and k_{β} :** As is visible in the simulation results the bound $k_{\beta, \text{rad}}$ obtained from Proposition 3 can be quite conservative in terms of the number of samples required to satisfy a constraint. This renders it impractical for robotic applications that require real-time optimisation. Moreover, if the obstacles and the robot are not ball-shaped, they would need to be placed inside a ball-shaped hull. This could be compared to obstacle padding which adds further slack into the approximation of the chance constraint. In comparison, as seen in the same numerical experiments, k_{β} from Eq. (7) provides a very good approximation of the real chance constraint, both in simulation and real-world

experiments. This is one of the main contributions of this work: showing that the heuristic, theoretically grounded when its assumptions hold, is also accurate in practice when those assumptions only hold partially, such as in an MPC setting.

3) *Online Planning (MPC)*: The online planning experiments correspond to a receding horizon/model predictive control (MPC) approach, where a new robot trajectory is planned at every MPC step $t_{i,\text{MPC}} = t_{i-1,\text{MPC}} + \Delta_{\text{MPC}}$ with $1/\Delta_{\text{MPC}}$ being the run frequency of the MPC controller. At each MPC step, the robot gets a position update of the M obstacles in the environment, which is assumed to be exact, *i.e.*, no measurement uncertainty. As in the offline planning experiment, we assume that CC-VPSTO has access to an accurate generative model that generates predictions of the future obstacle motions. In our online our online experiments we use a random walk model, parameterised to match the simulation environment. In a real-world setting, this could be replaced by a generative model learned from real-world data, *e.g.*, a model similar to [32]. In our optimisation scheme, given a position update, new obstacle trajectories are sampled from the random walk model and rolled out for a fixed time horizon $T > \Delta_{\text{MPC}}$. As described in Section VII-A, one particle in this experiment corresponds to one belief state of how the obstacles are going to evolve in the next time steps, *i.e.*, one particle maps to M trajectory predictions for M obstacles. Hence, when using N particles, we generate $M \cdot N$ obstacle trajectories, *i.e.*, the MC simulations, of duration T . At each MPC-step, after sampling these new trajectory predictions, we use them to re-run CC-VPSTO.

We evaluate online CC-VPSTO on four metrics across three environment configurations with four or five obstacles. Each obstacle is initialised with varying start position, velocity, and acceleration variance in the random walk model. The trajectory we evaluate is the trajectory that the robot executes, *i.e.*, the concatenation of the first Δ_{MPC} time steps of each of the solutions across MPC steps. One single experiment produces one trajectory from the initial position to the goal for the given environment instantiation and η -value. Fig. 6 shows three example rollouts and the respective CC-VPSTO solutions for different values of η for each of them. Note, that the length of the plotted obstacle rollouts was not fixed across the three examples, but depended on the maximum duration of the generated solutions for the given example. All solutions depicted are collision-free. Additional details about the configurations can be found in the appendix in Sec. E-A. For each environment configuration and for different values of η (0.05, 0.2, 0.4, 0.6, 0.8), we run 1000 experiments.

The evaluation metrics for the experiments are:

- 1) **Motion duration (time to until goal reached)**: This translates to the number of MPC-steps needed until the robot reaches the goal. In the experiments, we set a maximum number of 100 MPC steps. We only report the duration for successful experiments.
- 2) **Success rate**: The fraction of experiments, where the generated trajectory reaches the goal within the maximum number of MPC steps. An experiment is further only considered to be successful if the executed robot

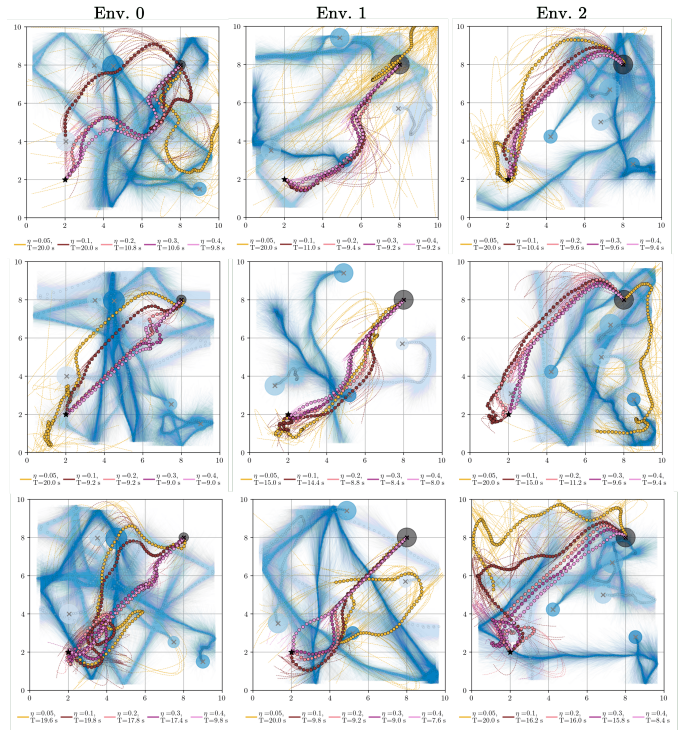


Fig. 6. *Overview of the environments used for the MPC experiments.* In each column, one per environment configuration, we show three examples of how the obstacle rollouts can look like, given the same environment configuration. The initial obstacle positions and their radii are shown by the blue circles. The smaller circles along the trajectories indicate the ground truth MPC updates, whilst the opaque trajectories plotted from each smaller circle show the particle predictions at that MPC-step. In addition, we plot the solutions of the online-CC-VPSTO controller for varying η -values. The start and goal is shown by the dark grey circle, which also reflects the robot radius, and the star, respectively. In addition, we plot the current solution for that MPC step, *i.e.*, the trajectory segment from the current robot position planned over a receding horizon, shown as dashed lines.

trajectory does not collide at any point of time with any of the obstacles *and* if the goal is reached.

- 3) **Collision rate**: This rate reflects the share of experiments where the respective trajectories were in collision at least once with any of the obstacles across the entire motion.
- 4) **Minimum distance to obstacles**: Per experiment, we measure the closest distance of the robot to any of the obstacles across the entire motion. This metric is only reported for successful experiments.

Note, that these metrics are different from the metrics used in the offline evaluation. This is because we aim to show the properties of the MPC trajectory given the guarantees from the offline experiments (which corresponds to a single MPC step in the online case).

We compare our approach to a baseline, “ML-VPSTO”, where ML stands for maximum likelihood. Instead of computing the probability of constraint violation based on particles, ML-VPSTO uses the same particles to compute mean obstacle trajectories and uses standard VPSTO to generate a solution that avoids these trajectories. In addition, running CC-VPSTO with $\eta = 0$ can also be seen as a baseline, as this is comparable to using a hard collision avoidance constraint within VPSTO. For all MPC simulation experiments, we assumed a replanning

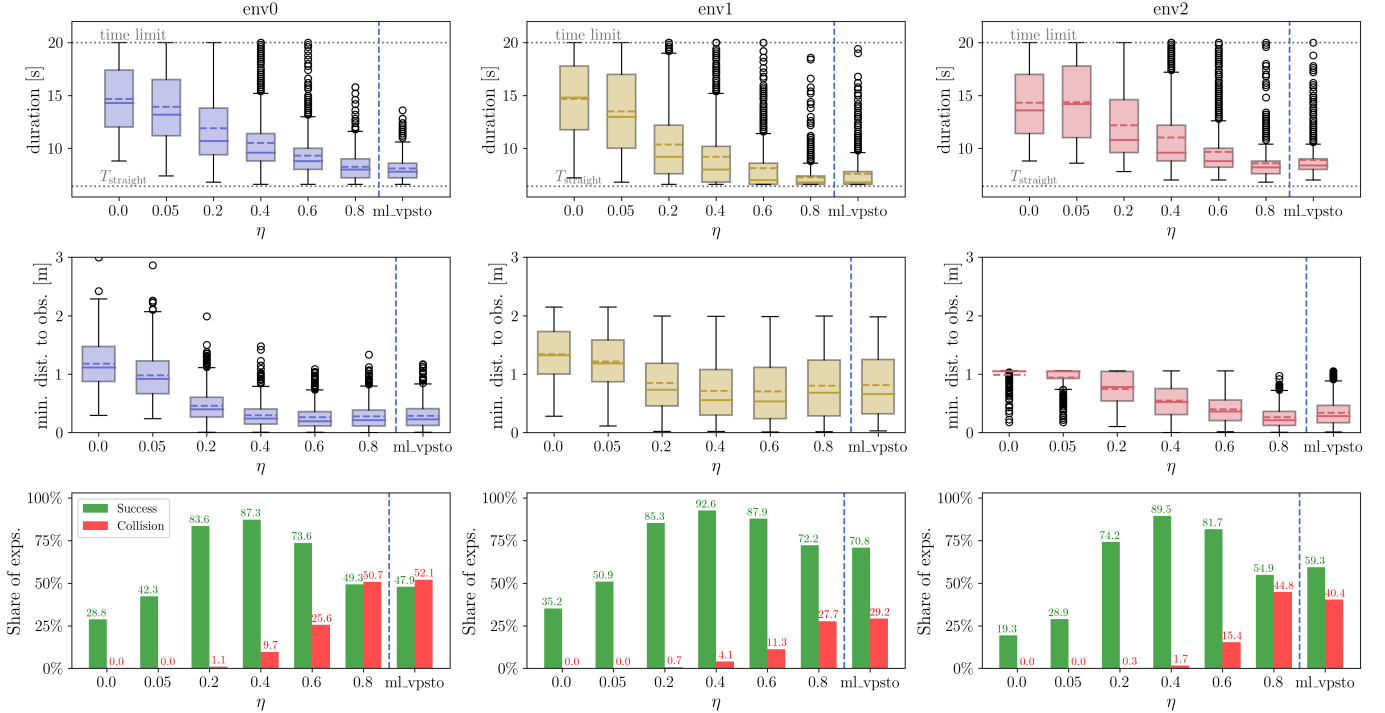


Fig. 7. **Simulation: MPC experiments.** Evaluating *motion duration*, *success rate*, *collision rate* and the *minimum distance to obstacles* across 1000 experiments on 3 different environments. One experiment corresponds to running online-CC-VPSTO until reaching the goal or until a maximum number of 100 MPC steps is reached. Goal and start location remain fixed across all experiments and environments, whilst the obstacle trajectories vary across experiments and environments. Each environment is initialized with different start positions and velocities of the obstacles, as well as different variance on the acceleration used in the random walk model. The boxplots include the mean (dashed line) and median (solid line) across all experiments.

frequency of 4 Hz, while setting the planning horizon T_{MPC} to 5 seconds (mapping to 100 time steps for the rollouts), the maximum number of MPC iterations to 100 and the number of particles N to 100.

Results: The results of the online experiment are a key insight of this paper, as they demonstrate the effects of combining *reactivity* (the MPC setting) with *safety* (the chance constraints). Fig. 7 summarises the results across the 1000 experiments for each of the 3 different environment configurations. We observe that CC-VPSTO in an MPC-loop is able to generate trajectories that are entirely collision-free for eta-values of up to 5%. In the given experimental setting, ML-VPSTO is approximately equivalent to permitting collisions with a probability as high as 80% in CC-VPSTO. In the most challenging environment configuration (env0) both approaches lead to a situation where 50% of the experiments are in collision. This indicates that employing average obstacle prediction for collision avoidance is inadequate, as a 50% collision rate is generally not an acceptable outcome in the majority of robotic applications. Moreover, the dependency of the safety/performance trade-off on the value of η is reflected in the motion duration. The higher the value of η , the shorter the duration of the trajectory. While ML-VPSTO produces the quickest trajectories, it is also the least safe approach. For reference, we also include T_{straight} in the duration plots, which is the duration of the straight-line trajectory from start to goal (ignoring obstacles). Last, when looking at the minimum distance to obstacles across trajectories and experiments, it seems like the expressiveness of this metric

depends on the environment configuration. For the first and second environment configuration, there is a decreasing trend, until it plateaus at values of $\eta > 0.4$ for the first environment. For the second environment configuration, after a downward trend, the minimum distance to obstacles increases again for values of $\eta > 0.4$. This can be explained by CC-VPSTO being more risk-taking and probably choosing a more direct path to the goal, which can possibly lead to more collisions, but in the case of no collision, the distance to obstacles might actually be bigger, as the motion is also quicker and some obstacles might not have had time to move closer to the robot. Last, the small variance in the distances for small η -values in the third environment can be explained by the initial configuration of obstacles, as they are already very close to the robot, which is then probably already the minimum distance across the entire motion. Overall, for this experiment setting, it seems like CC-VPSTO with $\eta = 0.4$ offers a good trade-off between safety and performance, as it is able to generate safe trajectories with a high success rate, whilst also being able to generate trajectories that are efficient in their motion duration.

C. Robot Experiment

We further demonstrate CC-VPSTO on a real robot for the scenario shown in Fig. 8. The robot is tasked to move from one side to the other of the conveyor belt, whilst avoiding a box which is controlled according to a stochastic policy. This requires the robot to be *reactive* whilst being able to plan *safe* motions in real time. The possible motions, also illustrated in Fig. 1, are to either move behind or in front of the box, as the

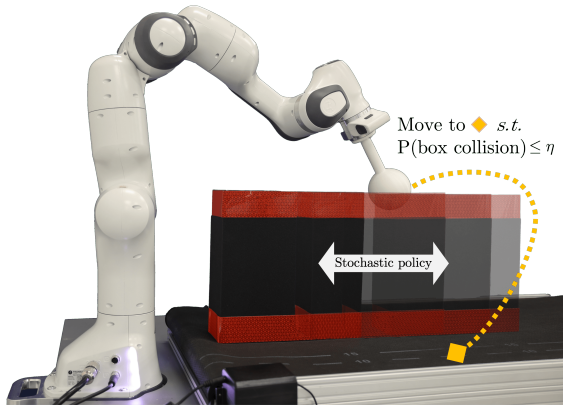


Fig. 8. **Robot experiment setup.** The robot task is to move from one side to the other side of the conveyor belt while assuring that the probability of colliding with the box obstacle is below a user-defined threshold η . The motion of the box obstacle is stochastic, as the conveyor belt is actuated with constant velocity, but the rate of direction change follows an exponential distribution.

robot is not allowed to simply move over the box. Moreover, besides the trajectories that we synthesise from the sampled via-points in CC-VPSTO, we also inject waiting trajectories into the optimisation, which are trajectories that do not move the robot at all. This is to allow the robot to wait for the box to pass, which is a safe, but not very efficient solution. Without these waiting trajectories, CC-VPSTO would keep the robot moving at all times, but this is not always necessary.

Setup. The experiment is performed on a Franka Emika robot arm. The framework was run on Ubuntu 20.04 with an Intel Core i7-8700 CPU@3.2GHz and 16GB of RAM. The ground truth box position is tracked using an Intel RealSense camera and a barcode detection pipeline. In every MPC step the robot is given the current position of the box and then plans a new trajectory using CC-VPSTO⁶. With this setup, we are able to run the framework at a frequency of 3 Hz, using $N = 100$ particles and a planning horizon of $T_{\text{MPC}} = 3$ seconds.

Stochastic conveyor belt policy. In this experiment, the uncertainty stems from the movement of the box on the conveyor belt, which serves as an obstacle for a robot to navigate around. The conveyor belt is velocity controlled, where the magnitude of the velocity is fixed to $0.05 \frac{\text{m}}{\text{sec}}$ but its direction is governed by the probability density function $f(x; \alpha) = \alpha \exp(-\alpha x)$, where the probability density where x is the time since the last direction change and α is a parameter influencing the rate of direction change. We describe our implementation of this stochastic model in more detail in the appendix in Sec. E-C.

Results: Similar to the MPC experiments in simulation, we evaluate our real-world robot experiment on *i)* the motion duration per run, *i.e.*, the time taken to go from one side of the conveyor belt to the other side, *ii)* the share of experiments that collide with the box, and *iii)* the minimum distance to the box across 70 runs for different values of η , as shown in Fig. 9. We do not compare our approach to “ML-VPSTO” as for the given stochastic model, the mean over the exponential distribution is not meaningful. However, we include $\eta = 0.0$ as a baseline, which corresponds to a VPSTO approach with

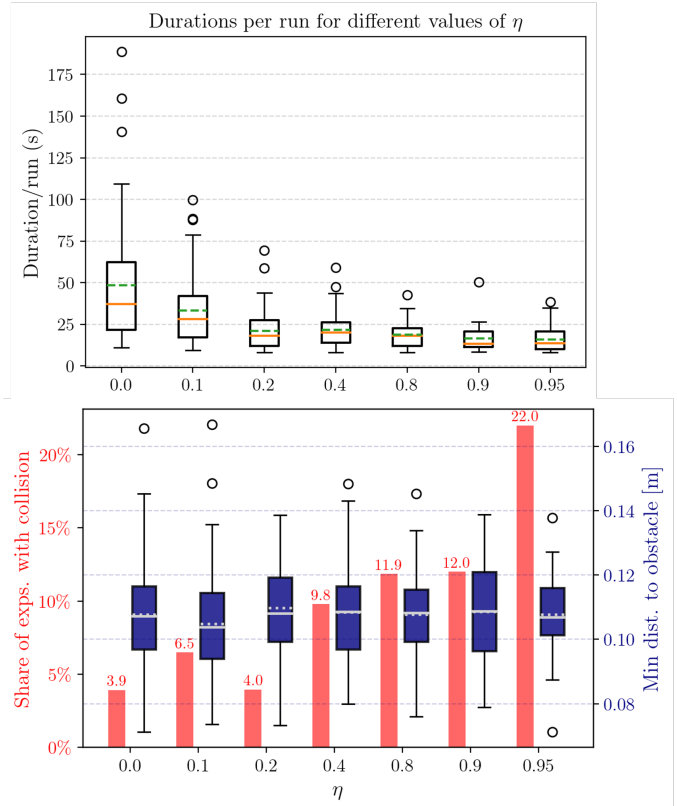


Fig. 9. **Robot experiment results.** Similar to the metrics evaluated in the MPC simulation experiments, we evaluate the *motion duration*, *minimum distance* to the box and the *share of experiments that collide* with the box across 70 experiments for different values of η . Means in the boxplots are shown as dashed lines and medians as solid lines.

a hard collision avoidance constraint. Overall, the results support the insights gained from the simulation experiments. We observe that the higher the value of η , the shorter the duration of the trajectory. This is because with higher values of η , CC-VPSTO is allowed to generate trajectories that are more efficient, but also less safe. Moreover, we also observe the trend that higher values of η indeed lead to a higher share of experiments that collide with the box. However, we also observe that the share of experiments that collide with the box is still very low, even for very high values of η . This is an interesting insight from combining MPC with chance-constrained trajectory optimisation. In addition, we observe in this experiment that a value of $\eta = 0.2$ outperforms $\eta = 0.1$ in terms of the share of experiments that collide with the box. We anticipate that additional experiments will reduce this variability, as the current variance in the results is still quite high. Last, in terms of the minimum distance to the box, we cannot observe a clear trend across different values of η . This can be explained by the use of waiting trajectories that do not move the robot at all. The robot can choose to wait very close to the box, which is a safe, but not very efficient solution. This results in higher durations, but not higher minimum distances.

VIII. DISCUSSION AND FUTURE WORK

Our experiments show that CC-VPSTO is able to generate task-efficient motions while consistently bounding the probability of constraint violation, *e.g.*, collision with stochastic

⁶Note we ignore measurement noise in this setup.

obstacles. While it is typically more challenging to deal with safety constraints over entire trajectories (as opposed to constraints per time step), our Monte–Carlo formulation allows us to do this in a straightforward way by simulating trajectories of the obstacles and the robot then checking for collisions between them at any time over a given horizon. This is made possible by the flexibility of our approach which makes no assumption on the distribution of the uncertainty, but only requires sampling access to it. Hence, this can also be a joint distribution across all sources of uncertainty, *e.g.*, several obstacles. Yet, note that this will not capture possible interactions during the execution, as the robot could possibly even influence these uncertainties, *e.g.*, humans moving away from the robot if the robot comes their way.

As anticipated by the theory, the collision rate in the experiments was consistently below the threshold η . Nevertheless, we observe a gap between the collision rate and the threshold η . This gap is much bigger in the online planning (MPC) than in the offline planning experiments. This can be explained by the fact that at each MPC step we optimise trajectories for a longer horizon than just the time steps that we actually execute on the robot. Hence, the anticipation of potential collisions in the future makes us more conservative, resulting in lower actual rate of collision than that which was imposed. In future work, we plan to use discounted probabilities in the chance constraint, such as in [18], to allow for larger probabilities of collision for time steps far in the future, knowing that the control input that we will apply then will be recomputed with stronger constraints in the meantime. Besides the introduction of discounted chance constraints, another direction could be to explore how to adapt the parameters η and β during online execution, *e.g.*, based on the current state of the system, the current uncertainty distribution, or the current cost function. This could result in a more robust and adaptive approach, which would be more suitable for real-world applications.

Another interesting direction for future research is about what to do in the case of an actual constraint violation, since we allow this with some probability. In our framework, since we do open-loop planning, there is no explicit way to deal with such cases. Implicitly in an MPC setting, we replan the motion given an update of the uncertain environment in the next MPC step. Yet, an interesting direction for future research is to explore closing the loop and switching the objective for the motion planner in the case of constraint violation. For instance, the objective could be turned into a purely safety maximizing formulation.

A core assumption in our approach is that we are given an *accurate* model of the uncertainty, from which we can take samples. Yet, this might be a limitation in practice, as our model might not capture the true underlying distribution with sufficient accuracy, relating to *epistemic uncertainty*. However, that can be addressed in future work, by either extending the approach to be *distributionally robust*, such as in [33], or by using generative data-driven models that can be adapted online as the robot acquires more data, similar to the work of Thorpe et al. [34].

In terms of computational efficiency, we have demonstrated the applicability of our algorithm to an MPC-setting, where

we achieve frequencies of 3 Hz on a real robot using 100 particles. The advantage of our formulation is that the user can actively choose the number of particles while considering computational resources and requirements of minimum control rates. We also believe that there is still room for improvement in our implementation, as the particle rollouts for the stochastic box model have not been parallelised, as was done in the simulation experiments. Possibly, replacing the Monte–Carlo simulations by a learned generative model from which predicted trajectories can be directly sampled could also lead to greater computational efficiency.

IX. CONCLUSION

In this work, we explored the problem of safe and efficient robot motion planning for stochastic control problems. We proposed a novel approach that combines the benefits of chance-constrained optimisation with the benefits of sampling-based MPC. The strength of our approach lies in its generality, as it does not require any specific assumptions on the underlying uncertainty distribution, the dynamics of the system, the cost function or the specific form of inequality constraints. While we focused on the problem of collision avoidance in this work, our approach is not limited to this problem, as it can be applied to any type of stochastic control problem, as long as we can sample from the uncertainty distribution. For instance, in future work we aim to extend this framework to include constraints on interaction forces in the context of contact-rich manipulation tasks and physical human-robot interaction. We showed that our approach is able to generate safe and efficient trajectories in a variety of scenarios, including a real-world robot experiment.

REFERENCES

- [1] A. Prékopa, *Stochastic programming*. Springer Science & Business Media, 2013, vol. 324.
- [2] S. Dai, S. Schaffert, A. Jasour, A. Hofmann, and B. Williams, “Chance constrained motion planning for high-dimensional robots,” in *2019 International Conference on Robotics and Automation (ICRA)*. IEEE, 2019, pp. 8805–8811.
- [3] K. Margellos, P. Goulart, and J. Lygeros, “On the road between robust optimization and the scenario approach for chance constrained optimization problems,” *IEEE Transactions on Automatic Control*, vol. 59, no. 8, pp. 2258–2263, 2014.
- [4] G. Schildbach, L. Fagiano, C. Frei, and M. Morari, “The scenario approach for stochastic model predictive control with bounds on closed-loop constraint violations,” *Automatica*, vol. 50, no. 12, pp. 3009–3018, 2014.
- [5] L. Blackmore, M. Ono, A. Bektassov, and B. C. Williams, “A probabilistic particle-control approximation of chance-constrained stochastic predictive control,” *IEEE Transactions on Robotics*, vol. 26, no. 3, pp. 502–517, 2010.
- [6] J. Jankowski, L. Bruder Müller, N. Hawes, and S. Calinon, “VP-STO: Via-point-based stochastic trajectory optimization for reactive robot behavior,” in *2023 IEEE International Conference on Robotics and Automation (ICRA)*. IEEE, 2023, pp. 10 125–10 131.
- [7] T. A. N. Heirung, J. A. Paulson, J. O’Leary, and A. Mesbah, “Stochastic model predictive control—how does it work?” *Computers & Chemical Engineering*, vol. 114, pp. 158–170, 2018.
- [8] A. Mesbah, “Stochastic model predictive control: An overview and perspectives for future research,” *IEEE Control Systems Magazine*, vol. 36, no. 6, pp. 30–44, 2016.
- [9] O. de Groot, L. Ferranti, D. Gavrila, and J. Alonso-Mora, “Scenario-based motion planning with bounded probability of collision,” *arXiv preprint arXiv:2307.01070*, 2023.

- [10] E. Schmerling and M. Pavone, “Evaluating trajectory collision probability through adaptive importance sampling for safe motion planning,” *arXiv preprint arXiv:1609.05399*, 2016.
- [11] L. Blackmore, “A probabilistic particle control approach to optimal, robust predictive control,” in *AIAA Guidance, Navigation, and Control Conference and Exhibit*, 2006, p. 6240.
- [12] G. C. Calafiore and M. C. Campi, “The scenario approach to robust control design,” *IEEE Transactions on automatic control*, vol. 51, no. 5, pp. 742–753, 2006.
- [13] G. C. Calafiore, “Random convex programs,” *SIAM Journal on Optimization*, vol. 20, no. 6, pp. 3427–3464, 2010.
- [14] G. O. Berger, R. M. Jungers, and Z. Wang, “Chance-constrained quasi-convex optimization with application to data-driven switched systems control,” in *Learning for Dynamics and Control*. PMLR, 2021, pp. 571–583.
- [15] A. Wang, A. Jasour, and B. Williams, “Moment state dynamical systems for nonlinear chance-constrained motion planning,” *arXiv preprint arXiv:2003.10379*, 2020.
- [16] S. Priore and M. Oishi, “Chance constrained stochastic optimal control based on sample statistics with almost surely probabilistic guarantees,” *arXiv preprint arXiv:2303.16981*, 2023.
- [17] L. Blackmore, H. Li, and B. Williams, “A probabilistic approach to optimal robust path planning with obstacles,” in *2006 American Control Conference*. IEEE, 2006, pp. 7–pp.
- [18] S. Yan, P. Goulart, and M. Cannon, “Stochastic model predictive control with discounted probabilistic constraints,” in *2018 European Control Conference (ECC)*. IEEE, 2018, pp. 1003–1008.
- [19] A. Nemirovski and A. Shapiro, “Convex approximations of chance constrained programs,” *SIAM Journal on Optimization*, vol. 17, no. 4, pp. 969–996, 2007.
- [20] A. M. Jasour, N. S. Aybat, and C. M. Lagoa, “Semidefinite programming for chance constrained optimization over semialgebraic sets,” *SIAM Journal on Optimization*, vol. 25, no. 3, pp. 1411–1440, 2015.
- [21] G. Alcan and V. Kyrki, “Differential dynamic programming with nonlinear safety constraints under system uncertainties,” *IEEE Robotics and Automation Letters*, vol. 7, no. 2, pp. 1760–1767, 2022.
- [22] M. Ono and B. C. Williams, “Iterative risk allocation: A new approach to robust model predictive control with a joint chance constraint,” in *2008 47th IEEE Conference on Decision and Control*. IEEE, 2008, pp. 3427–3432.
- [23] A. Parsi, P. Anagnostaras, A. Iannelli, and R. S. Smith, “Computationally efficient robust mpc using optimized constraint tightening,” in *2022 IEEE 61st Conference on Decision and Control (CDC)*. IEEE, 2022, pp. 1770–1775.
- [24] W. Sun, L. G. Torres, J. Van Den Berg, and R. Alterovitz, “Safe motion planning for imprecise robotic manipulators by minimizing probability of collision,” in *Robotics Research: The 16th International Symposium ISRR*. Springer, 2016, pp. 685–701.
- [25] J. Van Den Berg, P. Abbeel, and K. Goldberg, “Lqg-mp: Optimized path planning for robots with motion uncertainty and imperfect state information,” *The International Journal of Robotics Research*, vol. 30, no. 7, pp. 895–913, 2011.
- [26] J. Yin, Z. Zhang, and P. Tsiotras, “Risk-aware model predictive path integral control using conditional value-at-risk,” in *2023 IEEE International Conference on Robotics and Automation (ICRA)*. IEEE, 2023, pp. 7937–7943.
- [27] N. Hansen, “The CMA evolution strategy: A tutorial,” *arXiv preprint arXiv:1604.00772*, 2016.
- [28] M. Taboga, “Lectures on probability theory and mathematical statistics,” (*No Title*), 2017.
- [29] M. C. Campi and S. Garatti, “A sampling-and-discarding approach to chance-constrained optimization: feasibility and optimality,” *Journal of optimization theory and applications*, vol. 148, no. 2, pp. 257–280, 2011.
- [30] J. Jankowski, M. Racca, and S. Calinon, “From Key Positions to Optimal Basis Functions for Probabilistic Adaptive Control,” *IEEE Robotics and Automation Letters*, vol. 7, no. 2, pp. 3242–3249, 2022.
- [31] M. Mohri, A. Rostamizadeh, and A. Talwalkar, *Foundations of machine learning*. MIT press, 2018.
- [32] C. Jiang, A. Cornman, C. Park, B. Sapp, Y. Zhou, D. Anguelov, et al., “Motiondiffuser: Controllable multi-agent motion prediction using diffusion,” in *Proceedings of the IEEE/CVF Conference on Computer Vision and Pattern Recognition*, 2023, pp. 9644–9653.
- [33] A. Hakobyan and I. Yang, “Wasserstein distributionally robust motion control for collision avoidance using conditional value-at-risk,” *IEEE Transactions on Robotics*, vol. 38, no. 2, pp. 939–957, 2021.
- [34] A. Thorpe, T. Lew, M. Oishi, and M. Pavone, “Data-driven chance constrained control using kernel distribution embeddings,” in *Learning for Dynamics and Control Conference*. PMLR, 2022, pp. 790–802.
- [35] Z. Zhang, J. Tomlinson, and C. Martin, “Splines and linear control theory,” *Acta Math. Appl.*, vol. 49, pp. 1–34, 1997.
- [36] B. Gärtner and M. Hoffmann, “Computational geometry lecture notes hs 2013,” *Dept. of Computer Science, ETH, Zürich, Switzerland*, 2013.

APPENDIX

APPENDIX A

TRAJECTORY REPRESENTATION

The way we represent trajectories is based on previous work showing that the closed-form solution to the following optimisation problem

$$\begin{aligned} \min \quad & \int_0^1 \mathbf{q}''(s)^\top \mathbf{q}''(s) ds \\ \text{s.t.} \quad & \mathbf{q}(s_n) = \mathbf{q}_n, \quad n = 1, \dots, N \\ & \mathbf{q}(0) = \mathbf{q}_0, \mathbf{q}'(0) = \mathbf{q}'_0, \mathbf{q}(1) = \mathbf{q}_T, \mathbf{q}'(1) = \mathbf{q}'_T \end{aligned} \quad (12)$$

is given by cubic splines [35] and that it can be formulated as a weighted superposition of basis functions [30]. Hence, the robot’s configuration is defined as $\mathbf{q}(s) = \Phi(s)\mathbf{w} \in \mathbb{R}^D$, with D being the number of degrees of freedom. The matrix $\Phi(s)$ contains the basis functions which are weighted by the vector \mathbf{w} . The trajectory is defined on the interval $\mathcal{S} = [0, 1]$, while the time t maps to the phase variable $s = \frac{t}{T} \in \mathcal{S}$ with T being the total duration of the trajectory. Consequently, joint velocities and accelerations along the trajectory are given by $\dot{\mathbf{q}}(s) = \frac{1}{T}\Phi'(s)\mathbf{w}$ and $\ddot{\mathbf{q}}(s) = \frac{1}{T^2}\Phi''(s)\mathbf{w}$, respectively⁸. The basis function weights \mathbf{w} include the trajectory constraints consisting of the boundary condition parameters $\mathbf{w}_{bc} = [\mathbf{q}_0^\top, \mathbf{q}'_0^\top, \mathbf{q}_T^\top, \mathbf{q}'_T^\top]^\top$ and N via-points the trajectory has to pass through $\mathbf{q}_{via} = [\mathbf{q}_1^\top, \dots, \mathbf{q}_N^\top]^\top \in \mathbb{R}^{DN}$, such that $\mathbf{w} = [\mathbf{q}_{via}^\top, \mathbf{w}_{bc}^\top]^\top$. Throughout this paper, the via-point timings s_n are assumed to be uniformly distributed in \mathcal{S} . Note, that boundary velocities map to boundary derivatives w.r.t. s by multiplying them with the total duration T , i.e., $\mathbf{q}'_0 = T\dot{\mathbf{q}}_0$ and $\mathbf{q}'_T = T\dot{\mathbf{q}}_T$. Furthermore, the optimisation problem in Eq. (12) minimizes not only the objective $\mathbf{q}''(s)$, but also the integral over accelerations, since $\mathbf{q}''(s) = T^2\ddot{\mathbf{q}}(s)$ and thus the objective $\int_0^1 \ddot{\mathbf{q}}(s)^\top \ddot{\mathbf{q}}(s) ds$ directly maps to $\frac{1}{T^4} \int_0^1 \mathbf{q}''(s)^\top \mathbf{q}''(s) ds$, corresponding to the control effort. It is minimal *iff* the objective in Eq. (12) is minimal. As a result, this trajectory representation provides a linear mapping from via points, boundary conditions and the movement duration to a time-continuous and smooth trajectory.

CC-VPSTO, analogously to VP-STO, exploits this explicit parameterisation with via-points and boundary conditions by optimizing *only the via-points* while keeping the predefined boundary condition parameters fixed.

⁷A more detailed explanation of the basis functions and their derivation can be found in the appendix of [30].

⁸We use the notation $f'(s)$ for derivatives w.r.t. s and the notation $\dot{f}(s)$ for derivatives w.r.t. t .

TABLE I
MPC ENVIRONMENT SPECIFICATIONS

Env.	0	1	2
N_{obs}	5	4	5
Robot radius	0.25	0.5	0.5
\mathbf{x}_0	$\begin{bmatrix} 2.0 & 3.5 & 7.5 & 9.0 & 4.5 \\ 4.0 & 8.0 & 2.5 & 1.5 & 8.0 \end{bmatrix}$	$\begin{bmatrix} 7.9 & 1.3 & 4.9 & 5.2 \\ 5.7 & 3.5 & 9.4 & 3.0 \end{bmatrix}$	$\begin{bmatrix} 2.1 & 6.8 & 7.3 & 4.2 & 8.5 \\ 3.1 & 5.0 & 6.7 & 4.2 & 2.8 \end{bmatrix}$
$\dot{\mathbf{x}}_0$	$\begin{bmatrix} 0.7 & 0.25 & -0.5 & -0.1 & 0.0 \\ 0.0 & -0.5 & 0.5 & 0.1 & -1.0 \end{bmatrix}$	$\begin{bmatrix} 0.6 & 0.0 & -0.4 & -0.2 \\ 0.1 & 0.2 & 0.1 & 0.0 \end{bmatrix}$	$\begin{bmatrix} 0.5 & 0.5 & 0.0 & 0.4 & 0.2 \\ -0.2 & 0.0 & -0.2 & 0.6 & -0.3 \end{bmatrix}$
Radii	$[0.5, 0.4, 0.3, 0.35, 0.55]$	$[-0.32, 0.51, 0.49, 0.34]$	$[0.54, 0.45, 0.55, 0.35, 0.34]$
$var(\ddot{\mathbf{x}})$	$[0.5, 0.75, 0.65, 0.8, 0.6]$	$[0.54, 0.64, 0.51, 0.8]$	$[0.64, 0.66, 0.62, 0.57, 0.75]$

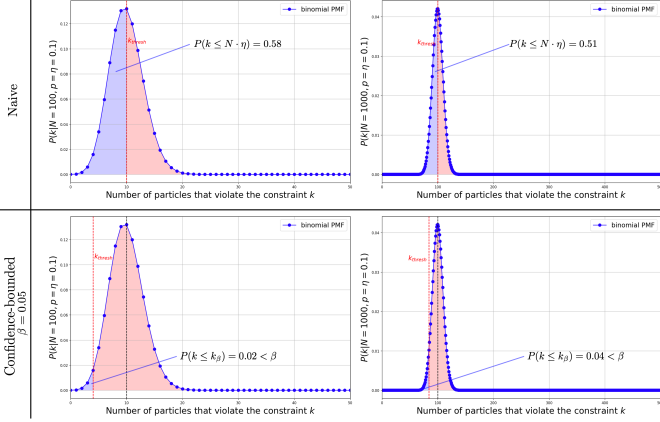


Fig. 10. Analysis of the binomial distribution with $N = 100$ (left column) and $N = 1000$ (right column) Bernoulli experiments, which correspond to the number of particles used to approximate the chance constraint in the optimisation. The top row shows the values k_{thresh} takes for the naive formulation of setting $k_{\text{thresh}} = \eta N$, where η is the user-defined maximum probability of violation. The bottom row shows the values k_{thresh} takes for the confidence-bounded formulation of the chance constraint, i.e., $k_{\text{thresh}} = k_{\beta} = C(k | N, p)^{-1}(\beta)$ for $\beta = 0.05$.

APPENDIX B

ADDITIONAL DETAILS ON NAIVE VS. CONFIDENCE-BOUNDED SURROGATE CONSTRAINT

We use Fig. 10 to illustrate the difference between the naive formulation that only considers the maximum violation threshold η by setting $k_{\text{thresh}} = \eta N$ and the confidence-bounded formulation using k_{β} . For this purpose we analyse the binomial distribution with parameters N and $p = \eta = 0.1$ for different values of N , which correspond to the number of particles $\delta_i \sim p_{\Delta}$ in the optimisation scheme. The plots in Fig. 10 shows the binomial distribution with $N = 100$ on the left and $N = 1000$ on the right. The blue shaded areas under the curve corresponds to the value of the CDF for k_{thresh} , i.e., $P(K \leq k_{\text{thresh}} | N, \eta)$. The red-colored area under the curve corresponds to the the probability that $k > k_{\text{thresh}}$. The top row shows the naive formulation, i.e., setting $k_{\text{thresh}} = \eta N$. The bottom row shows the confidence-bounded formulation, i.e., setting $k_{\text{thresh}} = C(k | N, p)^{-1}(\beta)$ for $\beta = 0.05$.

APPENDIX C

SUPPLEMENTARY MATERIAL FOR SEC. VI-A

A. Guarantees for separable constraints

Assume that the constraint $g(\mathbf{x}, \delta) \leq 0$ has the form $h_1(\mathbf{x}) \geq h_2(\delta)$ wherein h_1 and h_2 are real-valued functions and h_1 is continuous. Then, we have the following result:

Corollary 2. *Under the above assumption on g , if $\mathbf{x}_{\text{accept}}$ is such that the associated k in Eq. (5) satisfies $k \leq k_{\beta}$. Then, with confidence $1 - \beta$ w.r.t. the sampling of $\{\delta_i\}_{i=1}^N$, we can say that $\mathbf{x}_{\text{accept}}$ satisfies the chance constraint, i.e., $P(G_{\mathbf{x}_{\text{accept}}} = 1) \leq \eta$.*

This result is obtained as a corollary of Proposition 4 below, which states that a solution $\mathbf{x}_{\text{accept}}$ with $k \leq k_{\beta}$ does not satisfy the chance constraint only if some fixed solution $\mathbf{x}_{\text{fixed}}$ satisfies $k^{\text{fixed}} \leq k_{\beta}$.

More precisely, let $\mathbf{x}_{\text{fixed}}$ be such that $P_{\delta \sim \Delta}[h_2(\delta) > h_1(\mathbf{x}_{\text{fixed}})] = \eta$. With this definition of $\mathbf{x}_{\text{fixed}}$, we note that if $\mathbf{x}_{\text{fixed}}$ is rejected by the sample-based constraint, then any $\mathbf{x}_{\text{reject}}$ that violates the chance constraint will be rejected by the sample-based constraint as well:

Proposition 4. *Let $\mathbf{x}_{\text{reject}}$ be a solution that violates the chance constraint, i.e., such that $P(G_{\mathbf{x}_{\text{reject}}} = 1) > \eta$, and let $\{\delta_i\}_{i=1}^N$ be a set of N independent samples from p_{Δ} . A sufficient condition for $\sum_{i=1}^N P(G_{\mathbf{x}_{\text{reject}}} = 1 | \Delta = \delta_i) > k_{\text{thresh}}$ is that $\sum_{i=1}^N P(G_{\mathbf{x}_{\text{fixed}}} = 1 | \Delta = \delta_i) > k_{\text{thresh}}$.*

Proof. First, note that since $P(G_{\mathbf{x}_{\text{reject}}} = 1) > \eta$, and by definition of $\mathbf{x}_{\text{fixed}}$, it holds that $h_1(\mathbf{x}_{\text{reject}}) < h_1(\mathbf{x}_{\text{fixed}})$. Second, note that $\sum_{i=1}^N P(G_{\mathbf{x}_{\text{fixed}}} = 1 | \Delta = \delta_i) > k$ means that there are at least $k + 1$ samples δ_i such that $h_2(\delta_i) > h_1(\mathbf{x}_{\text{fixed}})$. Hence, there are at least $k + 1$ samples δ_i such that $h_2(\delta_i) > h_1(\mathbf{x}_{\text{reject}})$. Thus, $\sum_{i=1}^N P(G_{\mathbf{x}_{\text{reject}}} = 1 | \Delta = \delta_i) > k_{\text{thresh}}$, concluding the proof. \square

Since $\mathbf{x}_{\text{fixed}}$ is fixed, the variables $P(G_{\mathbf{x}_{\text{fixed}}} | \Delta = \delta_i)$ for $i = 1, \dots, N$, are independent. Hence, the conclusion of Corollary 1 applies, thereby providing Corollary 2.

B. Collision avoidance with separable constraints

In the context of safe robot motion planning, the constraint $h_1(\mathbf{x}) \geq h_2(\delta)$ can be used to impose collision avoidance with a stochastic obstacle, as follows: The idea is to choose a nominal point, denoted by \bar{p} (e.g., \bar{p} can be taken as the ‘‘center’’ of the current position of the obstacle), and obtain a bound d_{η} on the distance between the obstacle and \bar{p} that holds with probability $1 - \eta$ with respect to the uncertainty scenarios. We then plan a robot trajectory that not come closer than d_{η} to \bar{p} . This will ensure that with probability $1 - \eta$, the robot will not collide with the obstacle. More precisely, we let $h_2(\delta)$ be the maximal distance between \bar{p} and a point of the obstacle in scenario δ ; and $h_1(\mathbf{x})$ be the minimal distance between \bar{p} and a point of the robot in configuration \mathbf{x} (cf.

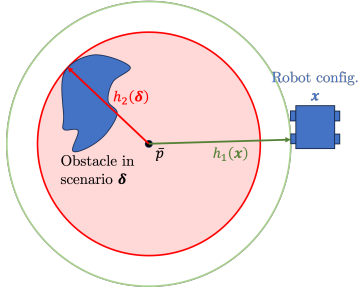


Fig. 11. Illustration of the constraint $h_1(\mathbf{x}) \geq h_2(\delta)$ to avoid collision between a stochastic obstacle and the robot. In the figure, $\bar{\mathbf{p}}$ is an arbitrarily chosen *nominal point*; $h_2(\delta)$ is the maximal distance between $\bar{\mathbf{p}}$ and any point of the obstacle in scenario δ ; and $h_1(\mathbf{x})$ is the minimal distance between $\bar{\mathbf{p}}$ and any point of the robot in configuration \mathbf{x} . The chance constraint in the optimisation of \mathbf{x} is that $P_{\delta \sim \Delta}[h_1(\mathbf{x}) < h_2(\delta)] \leq \eta$. Note that the choice of $\bar{\mathbf{p}}$ may influence the satisfiability of $P_{\delta \sim \Delta}[h_1(\mathbf{x}) < h_2(\delta)] \leq \eta$. In many cases (e.g., MPC), $\bar{\mathbf{p}}$ can be chosen as the “center” of the current position of the obstacle.

Fig. 11). Then, the robot avoids collision with the obstacle in scenario δ if $h_1(\mathbf{x}) \geq h_2(\delta)$. Our safety requirement is then that with probability $1 - \eta$ on δ , $h_1(\mathbf{x}) \geq h_2(\delta)$, i.e., $P_{\delta \sim \Delta}[h_1(\mathbf{x}) < h_2(\delta)] \leq \eta$. Note that this approach is interesting for short-term planning because the obstacles are likely to not move to far away from their current position. However, for longer horizons, the above planning strategy may become too conservative because the obstacles may wander far away from their initial position if they are given enough time. This would make the planning of a trajectory impossible, while there might still be a trajectory that avoids the obstacles with high probability.

APPENDIX D PROOFS OF SEC. VI-B

Proposition 5. *In the robotics setting defined in Sec. VI with $m = H = 1$, the Rademacher complexity of F can be bounded as follows:*

$$R_N(F) \leq \sqrt{\frac{d \log\left(\frac{eN}{d}\right)}{2N}}, \quad (13)$$

wherein $d = n + 1$ and e is Euler’s number.

Proof. The notion of Rademacher complexity is generally used in the context of learning classifiers from data. Thus, we reformulate our problem as a classification problem in order to apply known results on the Rademacher complexity. To do that, observe that for a given sample set $\{\delta_i\}_{i=1}^N$, any solution \mathbf{x} induces a classification of the samples into two categories: those that collide with \mathbf{x} and those that avoid \mathbf{x} . Furthermore, from the assumed nature of the problem, the classification induced by \mathbf{x} is a classification obtained by a “ball classifier”: indeed, the samples that collide with \mathbf{x} are exactly the samples for which $\mathbf{p}(\delta_i)$ is in a ball of radius smaller than r centered at $\mathbf{q}(\mathbf{x})$, thus this classification can be obtained from a ball classifier.

We obtain the desired Eq. (13) by combining a well-known result linking the Rademacher complexity of a classifier with a measure of its complexity called the *VC-dimension* [31, Corollary 3.18], with the results in [36, Section 15.5.2] bounding the VC-dimension of ball classifiers. \square

Proposition 6. *In the robotics setting defined in Sec. VI with general m and H , the Rademacher complexity of F can be bounded as follows:*

$$R_N(F) \leq mH \sqrt{\frac{d \log\left(\frac{eN}{d}\right)}{2N}}, \quad (14)$$

wherein $d = n + 1$ and e is Euler’s number.

Proof. Note that $F = \{\delta \mapsto \max_{o,t} P(G_x^{o,t} = 1 \mid \Delta = \delta) : \mathbf{x}\}$, wherein $G_x^{o,t}$ accounts for the collision with obstacle o at time t , and the maximum is over all obstacles o and all time steps t . Indeed, since we consider the *joint* probability of collision, we want G to be one if there is an obstacle o and a time step t such that the robot collides with o at time t . We now use a well-known property of the Rademacher complexity [31, Ex. 3.8] to obtain $R_N(F) = \sum_{o,t} R_N(F_{o,t})$ wherein $F_{o,t} = \{\delta \mapsto P(G_x^{o,t} = 1 \mid \Delta = \delta) : \mathbf{x}\}$. Since each $F_{o,t}$ accounts for the collision with one obstacle at one time step, we know that $R_N(F_{o,t})$ is bounded as in Eq. (13). By summing over o and t , we get the desired result. \square

APPENDIX E EXPERIMENT DETAILS

A. MPC Experiments: Environment Details

In this section, we provide additional details about the environments used for the MPC experiments in Section VII-B. We used three different environment configurations for which we generated the parameters randomly. Tab. I shows the specifications of the environments, i.e., the number of obstacles N_{obs} , the initial obstacle positions \mathbf{x}_0 , the initial obstacle velocities $\dot{\mathbf{x}}_0$, the obstacle radii and the variance of the obstacle accelerations $\ddot{\mathbf{x}}$, when sampling from a zero-mean Gaussian distribution in the random-walk model. The environment size was chosen to be consistent across all environments on a 10 by 10 grid.

B. Detailed Results on Offline-CC-VPSTO

The numeric results for the offline planning experiments are shown in Tab. II.

C. Robot Experiment: Implementation of Stochastic Model

In this section, we provide additional details about the implementation of the stochastic model for the robot experiment in Section VII-C describing the motion of the box obstacle on the conveyor belt. As our approach is Monte-Carlo-based, in every MPC-step we simulate the motion of the box obstacle for N_{sim} particles. The particles are initialised with the same position and velocity as the box obstacle at the beginning of the MPC-step. The particles are then propagated through the conveyor belt dynamics for the duration of the MPC-step. The conveyor belt dynamics are modelled as a probabilistic system, where the probability of changing direction increases over time. A particle at time step k is modeled by state vector $\mathbf{s} = [x_k, \dot{x}_k, p_k]$ where x_k is the position, \dot{x}_k is the velocity, and p_k is the probability of changing direction at time step k . The dynamics of this system for each time step Δt can be described as follows:

TABLE II
OFFLINE PLANNING EXPERIMENTS FOR $\beta = 0.05$

η	η_{rad}	η_{binom}	$\hat{\eta}_{\text{avg}}$	$\hat{\eta}_{1-\beta}$	$\hat{\beta}$
0.05	n/a	0.01	0.0218	0.0499	0.0497
	n/a	0.038	0.0393	0.0503	0.0539
0.1	n/a	0.04	0.0525	0.0936	0.0325
	n/a	0.084	0.0854	0.1012	0.0627
0.15	n/a	0.08	0.0934	0.1449	0.0375
	n/a	0.131	0.1322	0.1508	0.0572
0.2	n/a	0.13	0.1438	0.2060	0.0656
	n/a	0.178	0.1794	0.2010	0.0574
0.25	n/a	0.17	0.1842	0.2515	0.0535
	0.009	0.227	0.2288	0.2518	0.0638
0.3	n/a	0.22	0.2350	0.3068	0.0667
	0.059	0.275	0.2764	0.3005	0.0533
0.35	n/a	0.26	0.2755	0.3507	0.0517
	0.109	0.324	0.3251	0.3510	0.0578
0.4	n/a	0.31	0.3262	0.4053	0.0627
	0.159	0.374	0.3760	0.4029	0.0705
0.6	n/a	0.51	0.5282	0.6101	0.0754
	0.359	0.573	0.5748	0.6025	0.0683
0.8	0.158	0.72	0.7359	0.8053	0.0668
	0.559	0.778	0.7798	0.8024	0.0714

1) *Update the Probability of Direction Change:*

$$p_{k+1} = p_k \cdot (1 - \alpha) \quad (15)$$

where α is the rate at which the probability of a direction change increases over time.

2) *Determine the Direction Change:*

- Sample a random number r from a uniform distribution between 0 and 1.
- If $r < p_{k+1}$ or if the projected position $x_k + \dot{x}_k \Delta t$ is outside the boundaries of the conveyor belt, a direction change occurs.

3) *Update State based on Direction Change:*

$$\dot{x}_{k+1} = \begin{cases} -\dot{x} & \text{if direction change occurs} \\ \dot{x} & \text{otherwise} \end{cases} \quad (16)$$

$$p_{k+1} = \begin{cases} \alpha & \text{if direction change occurs} \\ p_{k+1} & \text{otherwise} \end{cases} \quad (17)$$

4) *Update Position:*

$$x_{k+1} = x + \dot{x}_{k+1} \Delta t \quad (18)$$

Therefore, the updated state vector after each time step is:

$$\mathbf{s}_{k+1} = [x_{k+1}, \dot{x}_{k+1}, p_{k+1}] \quad (19)$$

In summary, the above models the probabilistic dynamics of one box particle on the conveyor belt, where the direction of motion can change randomly influenced by the parameter α and the physical constraints of the system.